Meteoritics & Planetary Science 39, Nr 7, 1069–1088 (2004)
Abstract available online at http://meteoritics.org

Structure and impact indicators of the Cretaceous sequence of the ICDP drill core Yaxcopoil-1, Chicxulub impact crater, Mexico

T. KENKMANN,* A. WITTMANN, and D. SCHERLER

Institut für Mineralogie, Museum für Naturkunde, Humboldt Universität Berlin, Invalidenstrasse 43, 10115 Berlin, Germany
*Corresponding author. E-mail: thomas.kenkmann@rz.hu-berlin.de

(Received 25 August 2003; revision accepted 05 April 2004)

Abstract–As part of the ICDP Chicxulub Scientific Drilling Project, the Yaxcopoil-1 (Yax-1) bore hole was drilled 60 km south-southwest of the center of the 180 km-diameter Chicxulub impact structure down to a depth of 1511 m. A sequence of 615 m of deformed Cretaceous carbonates and sulfates was recovered below a 100 m-thick unit of suevitic breccias and 795 m of post-impact Tertiary rocks. The Cretaceous rocks are investigated with respect to deformation features and shock metamorphism to better constrain the deformational overprint and the kinematics of the cratering process. The sequence displays variable degrees of impact-induced brittle damage and post-impact brittle deformation. The degree of tilting and faulting of the Cretaceous sequence was analyzed using 360°-core scans and dip-meter log data. In accordance with lithological information, these data suggest that the sedimentary sequence represents a number of structural units that are tilted and moved with respect to each other. Three main units and nine sub-units were discriminated. Brittle deformation is most intense at the top of the sequence and at 1300–1400 m. Within these zones, suevitic dikes, polymict clastic dikes, and impact melt rock dikes occur and may locally act as decoupling horizons. The degree of brittle deformation depends on lithology; massive dolomites are affected by penetrative faulting, while stratified calcarenites and bituminous limestones display localized faulting. The deformation pattern is consistent with a collapse scenario of the Chicxulub transient crater cavity. It is believed that the Cretaceous sequence was originally located outside the transient crater cavity and eventually moved downward and toward the center to its present position between the peak ring and the crater rim, thereby separating into blocks. Whether or not the stack of deformed Cretaceous blocks was already displaced during the excavation process remains an open question. The analysis of the deformation microstructure indicates that a shock metamorphic overprint is restricted to dike injections with an exception of the so called "paraconglomerate." Abundant organic matter in the Yax-1 core was present before the impact and was mobilized by impact-induced heating and suggests that >12 km^3 of organic material was excavated during the cratering process.

INTRODUCTION

The 65 million year-old Chicxulub impact crater, located at the northern Yucatán Peninsula, Mexico, is buried beneath several hundred meters of post-impact Tertiary sediments. Because the crater has been formed in an area of active deposition, its interior morphology was protected from the effects of erosion. Thus, the study of this crater offers a unique opportunity to gain new insights on the nature of a pristine large impact crater. The goal of the Chicxulub Scientific Drilling Project (CSDP) was to recover, for the first time, a complete section through the annular trough of one of the three terrestrial multi-ring basins and to obtain a thick sequence of melt rock, ejecta deposits, and slumped blocks of the deformed crater floor. A major goal of the project was to better constrain the target lithology, chemistry, and degree of shock and to use these to constrain the environmental effects of Chicxulub.

The Yaxcopoil-1 (Yax-1) bore hole was drilled 60 km south-southwest of the center of the Chicxulub impact crater within the annular trough between the peak ring and the crater rim down to a depth of 1511 m (Fig. 1a). Drilling of the Yaxcopoil-1 bore hole was completed in February 2002. The technical supervision was provided by ICDP, GeoForschungsZentrum Potsdam (GFZ), and DOSECC (Drilling, Observation, and Sampling of the Earth Continental

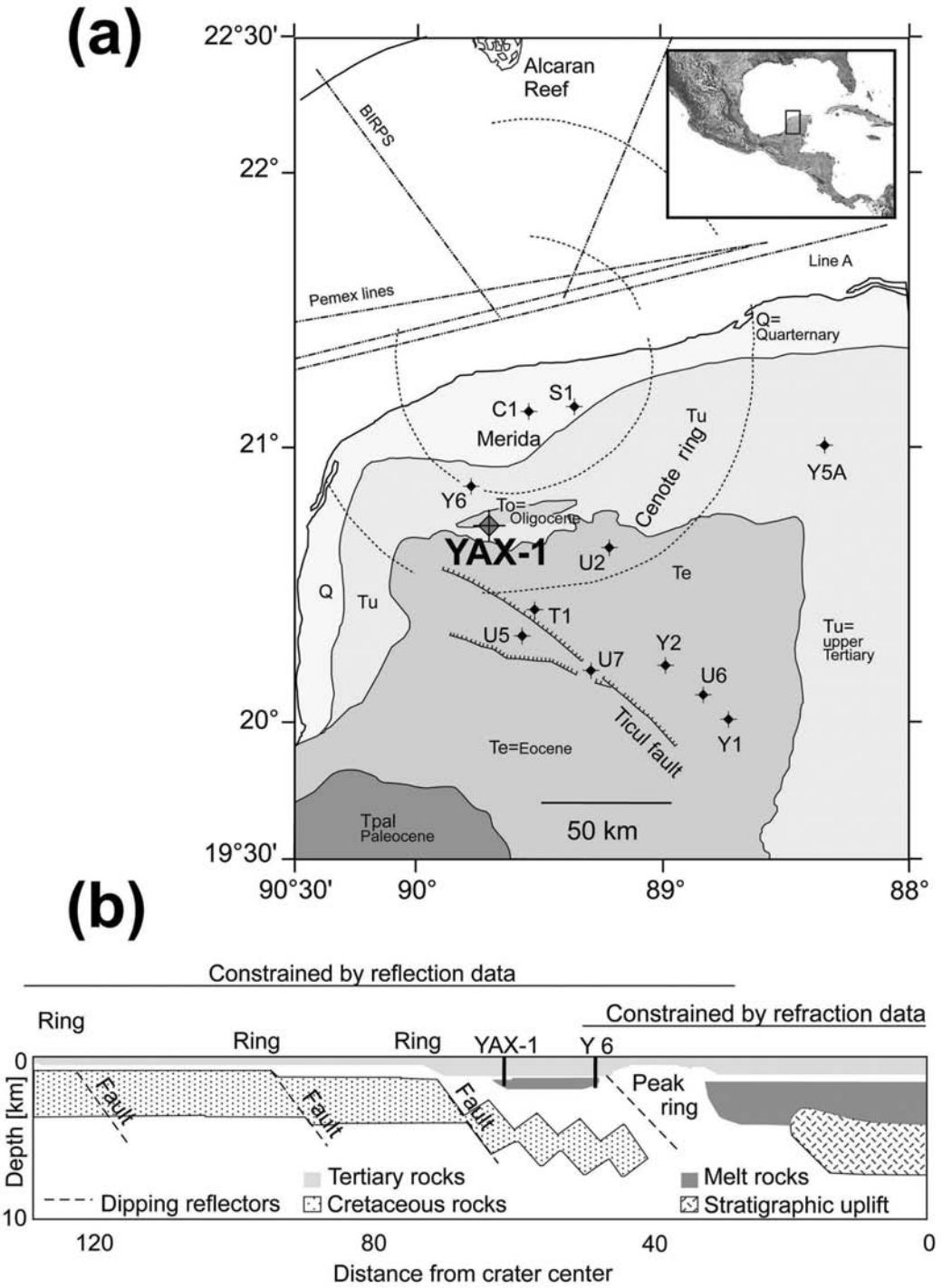

Fig. 1. a) Simplified geological map of the Chicxulub crater, northern Yucatán Peninsula, Mexico. Bore hole localities, seismic survey lines, and the main ring locations from gravity data after Sharpton et al. (1996) are additionally displayed; b) schematic cross section summarizing the main structural elements observed in the seismic data (redrawn after Morgan et al. [2000]).

Crust). The bore hole was completely cored from 404 m to 1511 m using the wireline coring technique (Dressler et al. 2003). The core is stored at the Universidad Nacional Autónoma de México (UNAM) in Mexico City.

From the results of the Yucatán-6 well (Y6), located at a distance of ~20 km from Yax-1 toward the center of the structure, as well as the Chicx-A seismic section (Morgan et al. 1997) and 3D gravity modeling (Ebbing et al. 2001), it was expected that several hundred meters of impact breccias would be encountered in the annular trough. After penetrating

795 m of post-impact sediments of Tertiary age and about 100 m of suevites and impact melt rock, 615 m of Cretaceous sediments were recovered. The Cretaceous rocks consist of dolomites, limestones, and anhydrites. Based on a biostratigraphic analysis, one age was determined near the base of the drill core at 1495–1455 m, where planktonic foraminifera were correlated with the Bonarelli event near the Cenomanian-Turonian boundary (Stinnesbeck et al. 2003).

For the structural analysis of the cores, a consideration of the spatial context of the bore hole Yax-1 is absolutely necessary. The knowledge of the internal structure of the Chicxulub crater mainly rests on seismic reflection studies (Fig. 1b) (Morgan et al. 1997, 2000; Hildebrand et al. 1998; Brittan et al. 1999; Morgan and Warner 1999; Christeson et al. 1999; Snyder and Hobbs 1999) and gravimetric data (Pilkington et al. 1994; Hildebrand et al. 1998). The dominant features in models of the Chicxulub crater are a collapsed central uplift of ~50 km-diameter with a ~18 km stratigraphic uplift (Christeson et al. 2001), covered by a ~3 km-thick and ~90 km-wide impact melt rock sheet (Pilkington et al. 1994). The collapse of the central rise led to the formation of a rugged peak ring with a 40 km radius that stands several hundred meters above the otherwise relatively flat crater basin floor (Brittan et al. 1999). The peak ring may consist of heavily brecciated material as indicated by a gravity low (Hildebrand et al. 1998; Morgan et al. 2000). The existence of slumped blocks beneath the peak ring and prominent inward dipping reflectors between the peak ring and the annular trough suggest a simultaneous outward collapse of the central uplift and inward collapse of the transient crater (Brittan et al. 1999). Hydrocode modeling of the crater collapse showed that the outward collapsing central rise overrides the overturned flap of the transient cavity rim. (Morgan et al. 2000; Kenkmann et al. 2000). The overridden overturned flap of the transient crater is supposed to define the outer limit of the peak ring. The bore hole locality is situated outside this peak ring in a zone where concentric structural elements of a distinct surface expression (Pope et al. 1996) and gravity signature (Hildebrand et al. 1998) are present. These are interpreted to be fault scarps and terraces formed by inward movements of the steep walls of the collapsing transient cavity. The 3D gravity model of Ebbing et al. (2001) had predicted, for the bore hole locality, a thin melt sheet of <<0.5 km at a depth of >1 km wedging out to the south-east and impact breccias of more than 1 km thickness beneath the melt sheet.

The east-west trending Chicx-A seismic section (Morgan et al. 1997) is usually projected radially into the plane defined by the crater center and the Yax-1 bore hole (Fig. 1b). Due to the approximate circular symmetry of craters, this radial projection is likely to show the principal structural features. However, it is not suited to exactly define lithological boundaries. Note that the distance of projection reaches more than 100 km in the outer areas of the section. Hence, it is not astonishing that drilling at Yax-1 did not penetrate through the thick breccia sequence exactly as suggested by the seismic data but encountered Cretaceous rocks.

It is supposed that large-scale movements had transformed the deep cavity to a shallow multi-ring structure with a double-sized diameter in comparison to the transient cavity. Using scaling laws, numerical models, and the geophysical data, the Chicxulub transient cavity size is estimated to be 90–100 km in diameter (e.g., Kring 1995; Morgan et al. 1997). Hence, the bore hole locality is placed outside the initial deep transient crater cavity.

Gravity data may suggest the existence of four different ring structures (Sharpton et al. 1996). The inner ring with 45–50 km radius and the third ring at about 90 km-radius distance are dominant (Fig. 1a). Presumably, the third ring represents the final crater rim. The structure terminates not with the crater's slumped rim but with a fault with a vertical offset of about 0.5 km transecting the whole crust and indicating the multi-ring nature of the structure (Melosh 1997).

To decipher the structural setting and modes of possible movements of the Cretaceous sequence during the cratering event, this paper will focus on the deformation overprint recorded in the rocks of the Yax-1 bore hole. For achieving a full understanding of the deformation history of the Cretaceous rocks, we analyzed the core with respect to: 1) the inclination and orientation of bedding planes; 2) the inclination and mode of faulting; 3) the degree of shock metamorphism; and 4) the deformation microstructure. The presented data are important to test the credibility of recent numerical models of the Chixculub impact, to understand the mechanics and kinematics of crater modification in large multi-ring impact craters, and, more generally, to derive modes of impact-deformation in stratified target rocks composed of carbonates and sulfates.

SAMPLE PREPARATION AND ANALYTICAL METHODS

For the analysis of the dip of bedding planes and faults, we systematically used the 360°-core scans of the Yax-1 core. The dip angle was calculated from the core circumference and the amplitude of a layer or fault, respectively. The core scans are not oriented; hence, it was impossible to derive the dip azimuth and to consider the deviation of the core axis from a vertical axis. Since the deviation never exceeds 2°, the latter can be neglected. We also used the Yax-1 dip-meter log data for correlation with the 360°-core scan data. In addition to the dip angle, dip-meter data also provide the azimuth of dipping. All geophysical log data used in this investigation were provided by ICDP, OSG (Operational Support Group), and GFZ-Potsdam.

Standard techniques were used to prepare samples. The preparation was particularly difficult due to residual stresses within the samples that caused severe fracturing. Some of the

samples, in particular those with dark brownish veins, reacted hygroscopically by taking up and retaining humidity. White-greyish needles of iron sulfates, most likely halotrichite crystals ($FeAl_2$ $[SO_4]_4$ * 22 H_2O), grew from these areas and reached cm size within a few days. Further growth was impeded by impregnation of the samples.

For optical and electron microscopy, we prepared doubly polished petrographic thin sections of 30 µm thickness. Most thin sections are oriented parallel to the drill core axis. Grinding and polishing procedures were performed with diamond saws and diamond paste, respectively. Clay-rich samples were treated with alcohol instead of water. Petrography, fabrics, and microstructures were studied using optical microscopy and a scanning electron microscope (JEOL JSM 6300) at 15 kV acceleration voltage coupled with an energy dispersive spectrometer (EDX) that allowed qualitative analyses of mineral phases. Quantitative structural investigations were performed using the LEICA Q-WIN image analysis package. For a fracture analysis (orientation, density, degree of localization), we digitized fractures from enlarged thin section photographs and used a skeleton procedure to isolate the fractures as lineations. This procedure also discriminates junction nodes where fractures transect or branch out. The number of nodes and the length of fracture segments between the nodes is a measure of deformation localization. The fracture density is given as cumulative fracture length in cm per cm^2. The orientation analysis shows the cumulative length of fractures in 10° bins.

RESULTS

Stratigraphy and Lithological Subdivision

A knowledge of the stratigraphy of the Cretaceous sequence of the Yax-1 bore hole is important to recognize and unravel possible deformational offsets and displacements. However, it is beyond the scope of this paper to provide a detailed lithological and sedimentological analysis. We used the lithological classification by Dressler (2002) and Dressler et al. (2003) for the lithological subdivision of the core. Deviations from this scheme are noted where necessary (Fig. 2). Interlayered units of calcarenite and anhydrite were resolved in our lithological profile if individual anhydrite layers exceed a thickness of 1 m. The resistivity log (Fig. 3) provided by ICDP/OSG/GFZ displays a good resolution of anhydrite layers, as they are characterized by high resistivities of >1000 ohm-m. Stinnesbeck et al. (2003) distinguished seven lithostratigraphic units within the Cretaceous sequence, which partly correspond to the subdivision given by Dressler et al. (2003): 1) 1495–1511 m: breccias with interlayers of dolostone and anhydrite; 2) 1455–1495 m: bituminous marly limestone; 3) 1315–1455 m: dolomite and minor anhydrite with breccia intervals; 4) 1155–1315 m: interlayered anhydrite, dolostone, and dolomitic limestone; 5) 1124–1155 m: chalky limestone; 6) 1040–1124 m: anhydrite, dolomite, and dolomitic limestone; 7) 894–1040 m: limestones, dolostones, peloidal packstones, and wackestones with foraminifera.

One biostratigraphic marker horizon was found by Stinnesbeck et al. (2003), defined by planktonic foraminifera at interval (2). It corresponds to the Cenomanian/Turonian boundary. Other than that, no unambiguous biostratigraphic constraints were found until now for the Cretaceous sequence. The lithostratigraphic record of the Cretaceous sequence also does not allow an unambiguous correlation with stratigraphic horizons of the undeformed Yucatán platform. Stratigraphy, therefore, is not suited to infer the degree of sediment deformation. It even remains uncertain whether the entire sequence or parts of it are not in an upside-down position.

Fractures, Faults, and Inclined Bedding Planes

Fracturing, faulting, and brecciation is a widespread phenomenon in the Cretaceous sequence. The variation of intensity of cataclasis is considerable (Fig. 2). A pronounced concentration of deformation and fracturing occurs near its top at depths of 900–920 m, 1000–1100 m, and at 1310–1400 m. The sonic log (ICDP/OSG/GFZ) (Fig. 3) reflects this concentration of fractures in so far as a remarkable scattering in sonic velocity with high amplitudes occurs at these intervals (Fig. 3).

Tilting

The inclination of bedding planes was measured along the entire Cretaceous sequence using the 360°-core scans (Fig. 2). The results show similar excursions as the dip-meter log data, which are available for the depth interval 965–1511 m (Fig. 2). Notwithstanding some discrepancies, the general trend coincides for both methods and indicates the reliability of the dip-meter data. The dip-meter log provides additional information on the dip direction. Regarding the dip inclination, a rough subdivision of the Cretaceous sequence into three major structural units is possible: a) 894 m–1142 m, b) 1142 m–1411 m, c) 1411 m–1511 m.

Interval (a) shows an average inclination of 36° ± 17° based on 360°-core scan measurements, but the scattering is large (Figs. 2, 4a, and 4b; Table 1). Below the suevitic dikes (Fig. 5a) at 916 m, a near-vertical position of layers can be inferred (Fig. 4b). The dip azimuth changes with depth. At the base of unit (a), the dip orientation is consistently toward the south-east; above 1050 m, layers are inclined toward the center of the crater (north-northeast). At the top of the unit, the inclination is toward the west (Fig. 2). It is unclear whether a gradational transition between the southeast, north-northeast, and west dipping sub-units exists. If so, the pattern could be explained by an asymmetric fold with a north-northeast plunging fold axis and a west-northwest dipping fold plane.

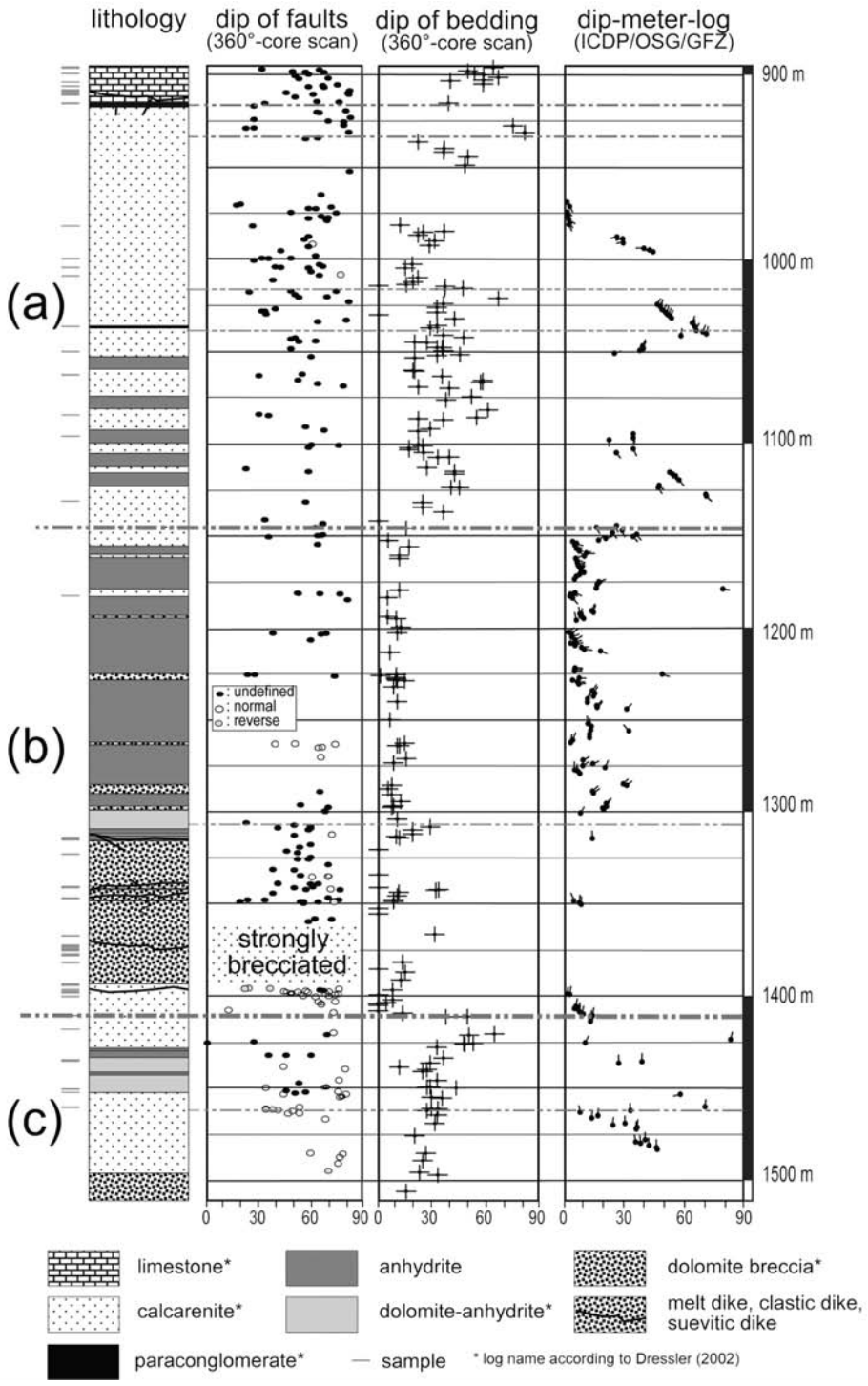

Fig. 2. Lithological profile of the Cretaceous sequence of the Yax-1 borehole. The columns show the dip of faults and the dip of bedding planes measured at the 360°-core scan images. The right column displays the dip-meter log data as provided by ICDP/OSG/GFZ-Potsdam. The marker lines indicate the depth of potential structural unit boundaries as discussed in the text.

However, it is more likely that the described sub-units of different azimuth are offset by faults. Within a single sub-unit, the dip-meter data gradationally decrease from foot wall to hanging wall in certain intervals, e.g., at 1025–1040 m, thereby indicating a bending and folding of the sub-units.

Unit (b) (1142–1411 m) generally shows a sub-horizontal or low-angle dip (mean: 9.9° ± 7.6°) (Fig. 2; Table 1). Occasionally, dipping reaches ~30°. The dip-meter data display a stronger scattering, which is due to an increasing error of azimuth data with decreasing dip angle. Alternatively,

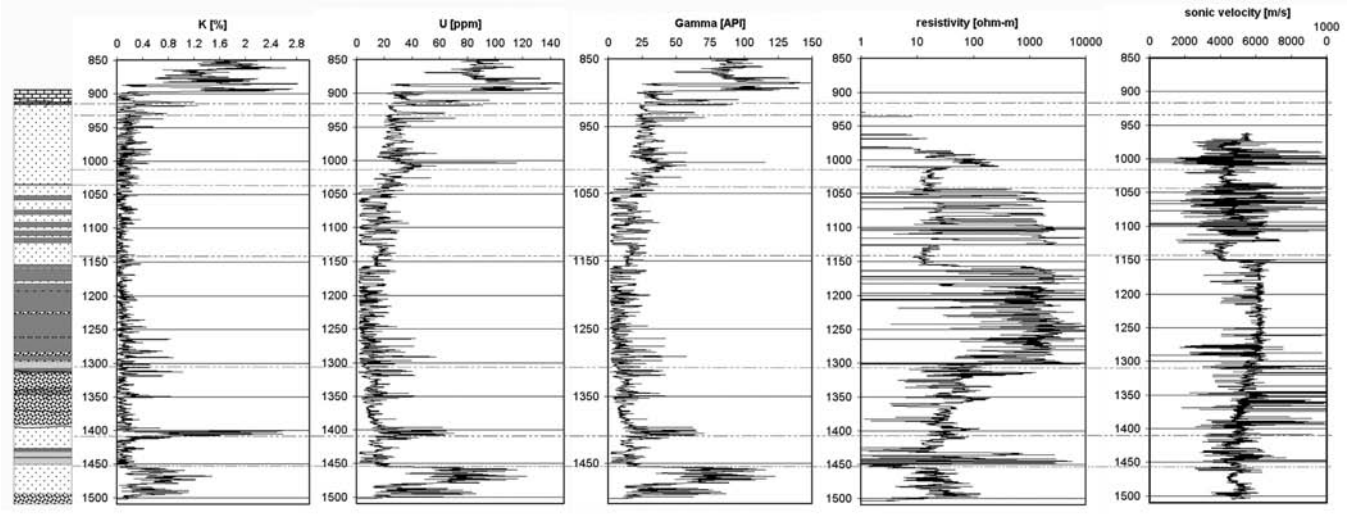

Fig. 3. Correlation of geophysical log data (ICDP/OSG/GFZ-Potsdam) with the lithological profile (left). The columns display (from left to right): K content in wt%, U content in ppm, gamma radiation in API, resistivity in ohm-m, and sonic velocity in m/s.

Table 1. Mean inclination of main structural units based on the analysis of 360°-core scans.

Structural unit	Depth interval (m)	Mean inclination (°)	Standard deviation (°)
(a)	936–1150	36.0	16.7
(b)	1150–1410	10.0	8.6
(c)	1410–1511	32.3	11.0

the scattering of the dip angle at short distances can be attributed to primary and secondary sedimentary features, e.g., the non-horizontal deposition of sediments in a sabkha and shallow marine environment, the gypsum-anhydrite dehydration with subsequent growth of nodular anhydrite (chicken-wire structures), and may be due to local solution phenomena. The lower part of this unit is heavily deformed and intruded by dikes.

Structural unit (c) (1411–1511 m) shows a steeper inclination (mean: 33.5° ± 11.6°) (Fig. 2; Table 1). Near the top of this unit, tilting locally reaches 60°. The tilt direction is toward the crater center (north).

The predominant mechanical decoupling horizons, which also correlate with lithostratigraphic changes (Stinnesbeck et al. 2003), most likely occur at 1142 m and at 1411 m. Based on the log data of Fig. 2, further subdivisions of these three main structural units into 9 sub-units are possible, and Fig. 5 displays some of the proposed structural boundaries between them: 1) 894 m–916 m: this unit is tilted by 45–60°, it is overlain by suevitic breccias and underlain by suevitic dikes (Fig. 6a). The latter may have acted as a decoupling horizon; 2) 916 m–~934 m: strongly inclined unit, but the lower boundary cannot be clearly defined; 3) ~934 m–~1014 m: possibly bent block dipping with 30–45° west; 4) ~1014 m–1038 m: bent block dipping with 45–65° north-northeast. According to Dressler's log description, a paraconglomerate layer exists in this section. The meaning of the so called "paraconglomerate" (Fig. 5a), which is, in fact, a diamictite that contains shocked quartz and allogenic fragments, is discussed in the Impact Indicators and Discussion sections. The proposed base of the unit is located below the diamictite; 5) 1038 m–1142 m: moderately inclined sequence dipping to the southeast. The base is defined by a zone of closely-spaced horizontal core breakthroughs and a green colored, foliated shear plane (Fig. 5b); 6) 1142 m–~1308 m: relatively flat lying unit composed of anhydrites interlayered with carbonates. Figure 5c displays the fault breccia of the lower boundary; 7) 1308 m–1411 m: strongly brecciated unit in which stratification is barely seen. The entire zone is disintegrated. All discovered polymict, clastic dikes, and impact melt dikes occur in this strongly deformed zone (Figs. 6b–6e); 8) 1411 m–1461 m: moderately to steeply inclined unit dipping to the north. A strong positive spike in resistivity (Fig. 3) marks the base of this unit. Discordances across a dark layer (Fig. 5d) and a concentration of reverse faults (Figs. 2 and 5e) occur at the base of this unit; 9) 1461 m–1511 m: folded unit dipping to the north.

It was partly difficult to define exact boundaries between the structural units because shear zones and decoupling horizons may be obscured by later sealing with carbonates and subsequent recrystallization. It was found that horizontal, narrow-spaced core breakthroughs may correlate with the proposed structural boundaries, e.g., at 1038 m or 1142 m (Fig. 5b). They indicate higher fracture densities that lead to a preferential failure during coring and stress relaxation.

The most plausible explanation for the existence of different intervals with different mean inclinations and dip orientations, which also considers the geological context of the bore hole locality within the crater, is that these different structural units and proposed sub-units reflect individual

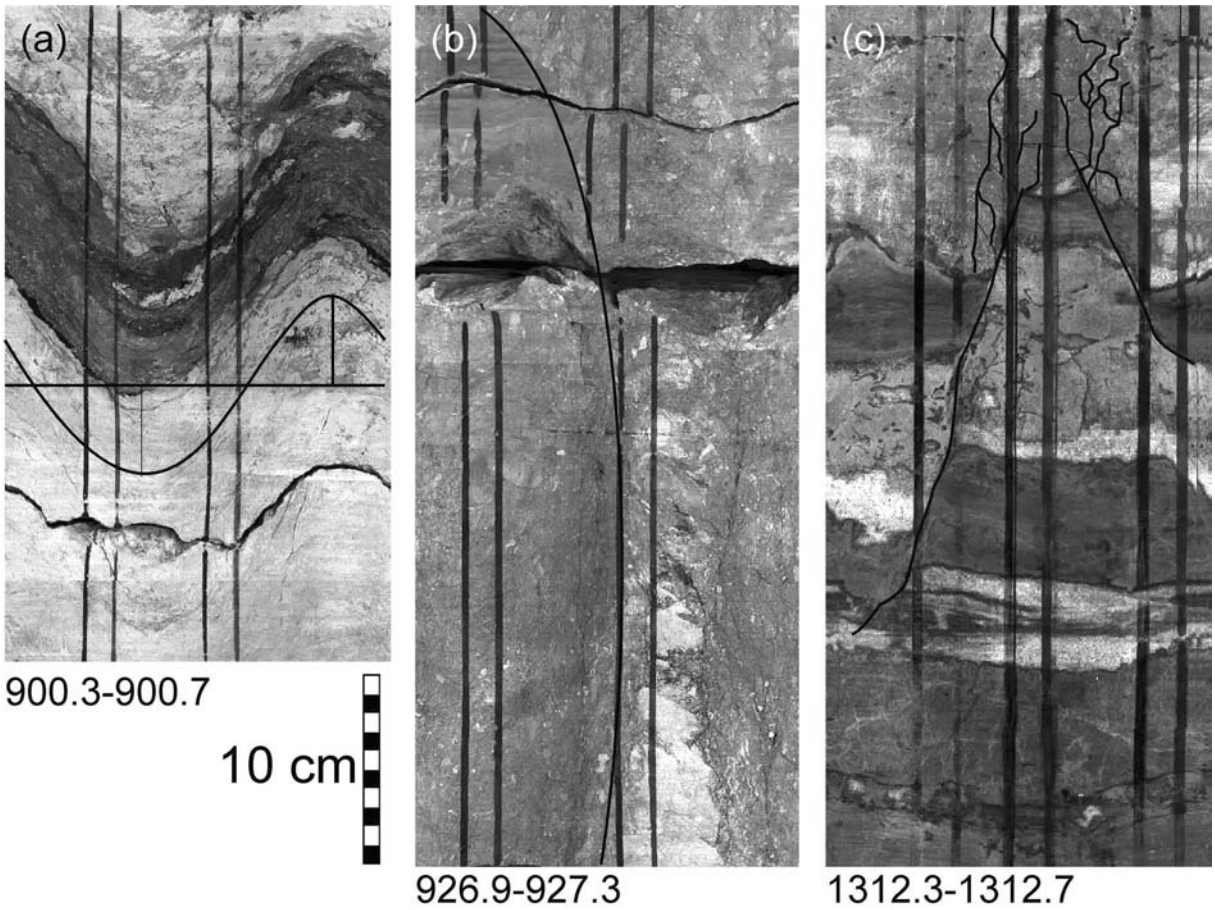

Fig. 4. 360°-core scan images. The dip angle, α, of a layer is calculated from the core circumference, U, and the amplitude, A, making use of the formula: $\tan \alpha = 2\pi A/U$; a) the layers are tilted by ~68°; b) below the suevitic dikes at 916 m, layers are occasionally in a sub-vertical position; c) normal faulting as it is displayed in the 360°-core scans. Measurement of dip angles of fault planes is the same as for bedding planes. Note that the normal faults are localized within the stratified anhydrite-limestone sequence and distributed in the massive dolomite (top).

blocks that were slightly bent internally and tilted against each other during a deformation event.

Faulting

Faults and fractures were investigated using the 360°-core scan images (e.g., Fig. 4c) and thin sections. A pronounced concentration of fractures and faults occurs near the top of the succession and at 1310–1400 m. Figure 2 displays the inclination of fault planes with depth. Many of the faults are undefined with respect to shear sense. Their average dip is 57° ± 17°. For those faults for which it was possible to derive a shear sense, normal faults clearly dominate over reverse faults. The former show dip angles of 65° ± 13°; the latter are dominantly thrusts with dips of 40° ± 18°. The visible off-sets are commonly small (e.g., Fig. 4c). A passive rotation of faults by a later tilting of blocks cannot be derived for the different structural units and sub-units from the logging data.

Lithological Dependencies of Faulting

The intensity of faulting and the geometry of faults is lithology dependent (Fig. 4c). Penetrative and interconnected shear zone networks have been formed within massive dolomitic rocks (Fig. 7). Strain is partitioned into shear zone networks with relatively small magnitudes of displacement on each fault. The bulk strain that can be accommodated by this type of distributed, delocalized faulting is estimated to be on the order of 20–30%. These rocks have the highest fracture density (Fig. 7). Faults and fractures have the tendency to scatter in orientation and to split in numerous small shear zones in these rocks. In contrast, stratified calcarenites, dolomites interlayered with anhydrites, and bituminous layered limestones are mainly disrupted by larger and more localized faults with strong grain size reduction and comminution occurring on fault planes. The scattering in fault orientation, the number of fault embranchments per cm, and the average fracture density is lower in these rocks in comparison to the massive dolomites (Fig. 7).

Massive anhydrites display nearly no macroscopically visible shear zones in the 360°-core scans. They were partly

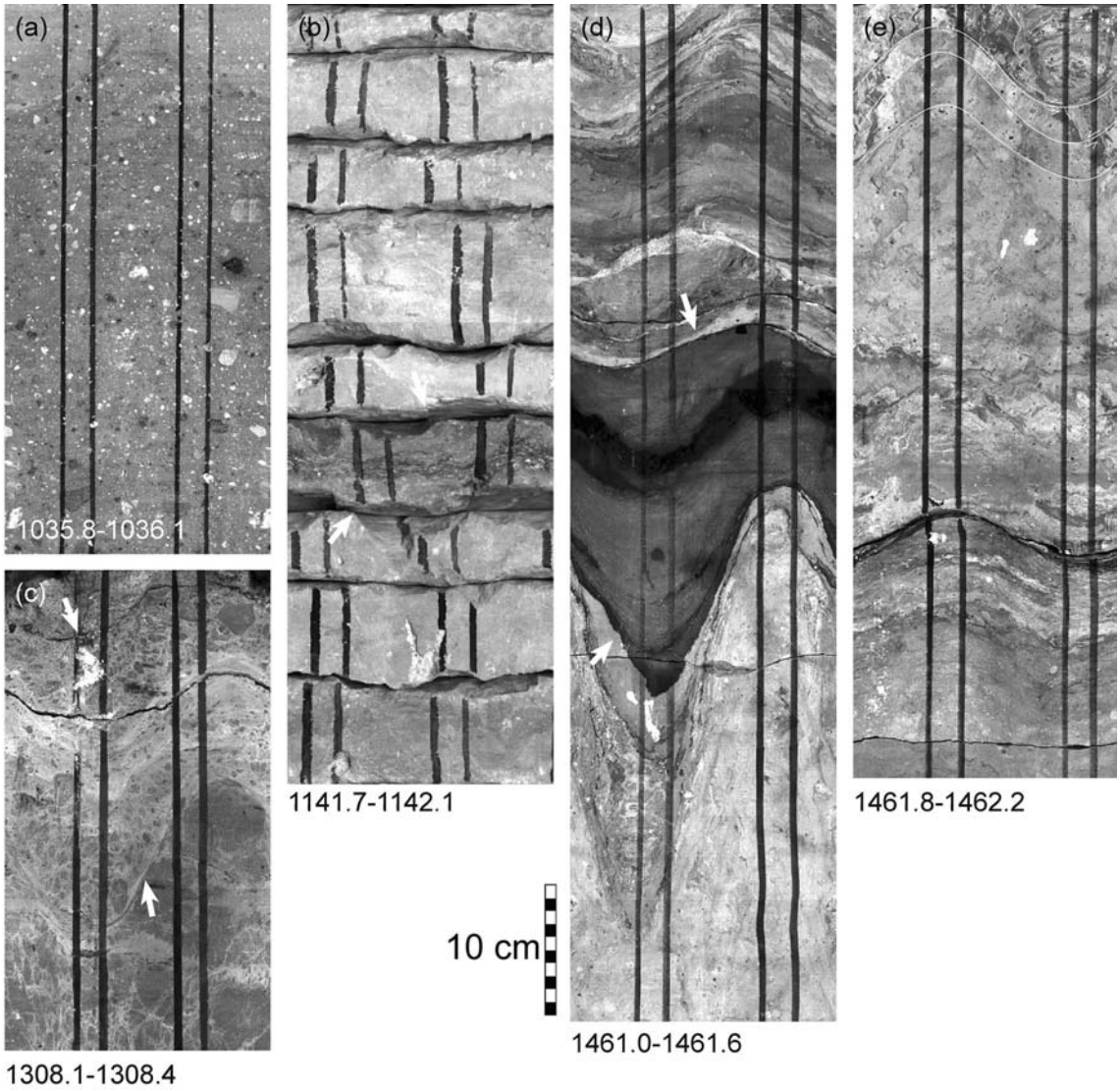

Fig. 5. 360°-core scan images of potential decoupling horizons: a) the so called "paraconglomerate" contains shocked minerals. Its origin as a diamictite or as a breccia is debated in the text; b) horizontal core breakthroughs are frequent at the proposed decoupling horizons. The green colored middle section (indicated by arrows) is a shear plane; c) the occurrence of a fault breccia and discordant lithological contacts indicate the disruption of the sequence at 1308 m; d) a steep angle discordance and a potential shear plane correlate with a layer enriched in organic matter; e) about one meter below the discordance of (d), sliding on bedding planes occurs.

sealed and, thereby, obscured. At higher resolution at the scale of thin sections, however, many faults can be traced through anhydrite nodules and layers (Fig. 8). Figure 8b, for instance, shows brittle fault zones cutting through an anhydrite nodule and deforming large euhedral anhydrite crystals cataclastically. This cross-cutting relationship clearly demonstrates that the formation of faults and breccias was not caused by an anhydrite-solution-induced collapse scenario as proposed by Stinnesbeck et al. (2003).

Impact-Induced versus Endogenic Faulting

Faults can be described by characteristic ratios of shear displacement (D) to fault thickness (T) and to fault length (L). Although not proven yet, the ratios of impact-induced and tectonic fault zones are likely to be different (e.g., Kenkmann 2002) because impact-induced faults are formed as single-slip, high strain events in contrast to their multi-incremental endogenic counterparts. In a first analysis, we have measured the ratio of fault displacement (D) and fault thickness (T) of the sample Yax-1_1399.05 m (Fig. 9). The D/T ratio does not deviate strongly from those of tectonic shear zones, but the gouge zones appear relatively thick with respect to the measured displacements. Anomalous thick gouge zones are favored by a highly damaged state of rock due to dynamic shock loading before shear zone formation. Alternatively, they indicate oscillating movements on fault planes, which lead to thick gouge zones but relatively minor visible offsets.

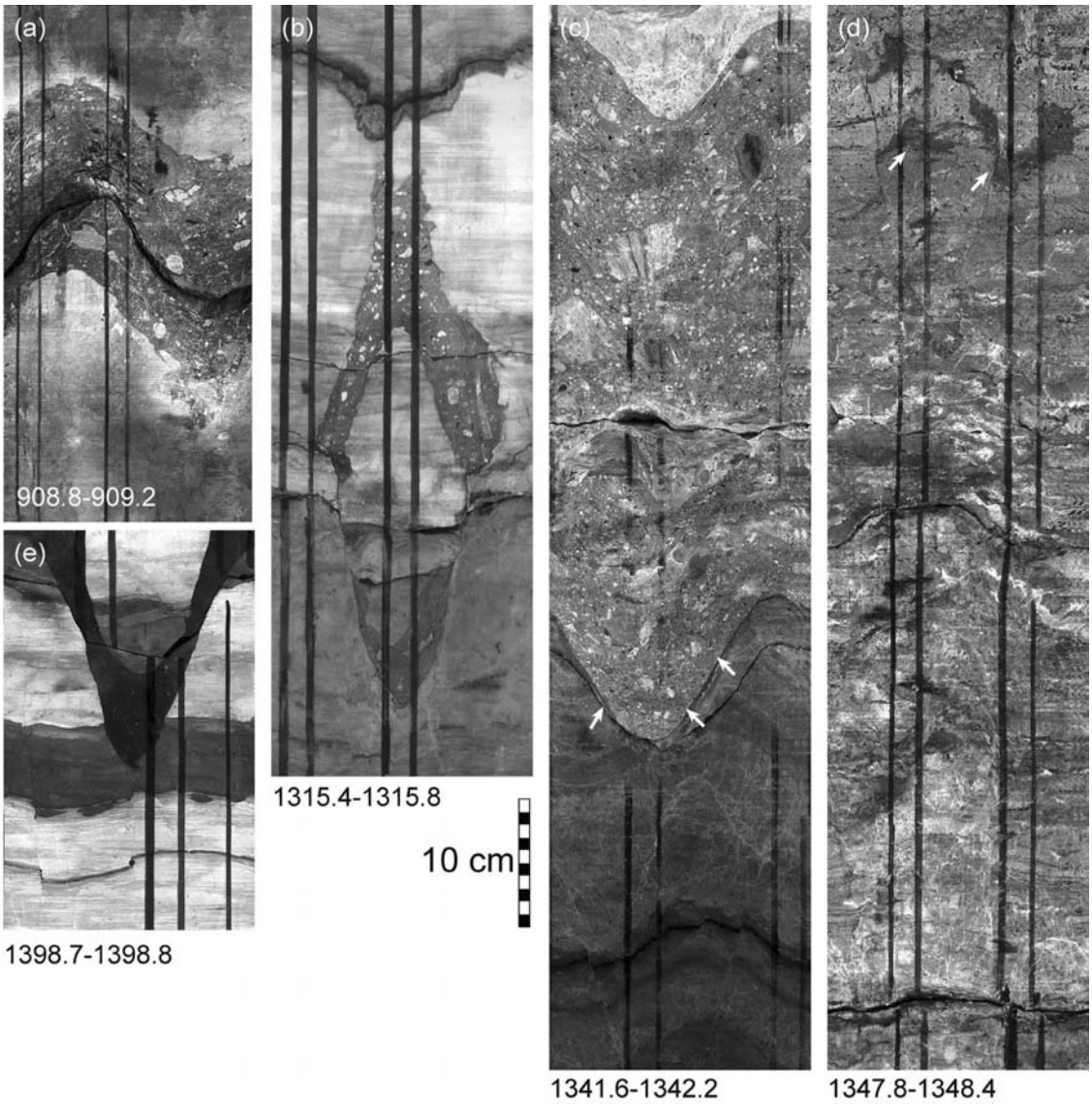

Fig. 6. 360°-core scan images of dike systems of the Yax-1 bore hole: a) the upper suevite dike is only 8 cm thick; b) the clastic polymict dike system at 1314–1316 m crosscuts the anhydrite-dolomite stratification nearly vertically; c) the polymict clastic dike at 1341–1342 m crosscuts the stratification obliquely; d) the impact melt rock dike shows ductile flow features in impact melt rock (arrows) that are offset by vertical faults. The surrounding of the melt flow features consists of fine- to coarse-grained, euhedral dolomite; e) the dark colored clastic dike at 1398–1399 m is associated with numerous normal faults that have formed syngenetically with the dike emplacement. The dark color is due to organic matter that afterward migrated into the porous matrix of the dike.

Time of Faulting

The formation of suevitic and polymict, clastic dikes can clearly be attributed to the Chicxulub impact event. Figures 6b, 6e, and 10 show that faults are frequent near the dikes and partly form parallel to the dike boundaries. Hence, they formed co-genetically with the dikes. Even though it is not justified to extrapolate this observation to the entire set of faults observed in the Cretaceous sequence, it gives a strong hint that many, if not most, of the faults are related to the impact. A few faults and fractures transect the dikes. The earliest moment of formation of these fractures is after the dikes became cohesive enough to be affected by brittle failure.

Faults displace the impact melt veins at 1347–1348 m (Fig. 11). This cross-cutting relationship points toward a formation time after the emplacement of the melt veins. However, the sheared impact melt reacts viscously and is partly smeared along the fault planes (Figs. 11b and 11c), suggesting a short hiatus between both events.

Mobilization of Organic Matter

Black and dark brownish stratiform layers in limestones, calcarenites, and dolomites (Figs. 5d, 7, 10, and 12), as well as dark coatings around anhydrite nodules (Fig. 8a), are zones enriched in organic matter. Most of the stratiform layers

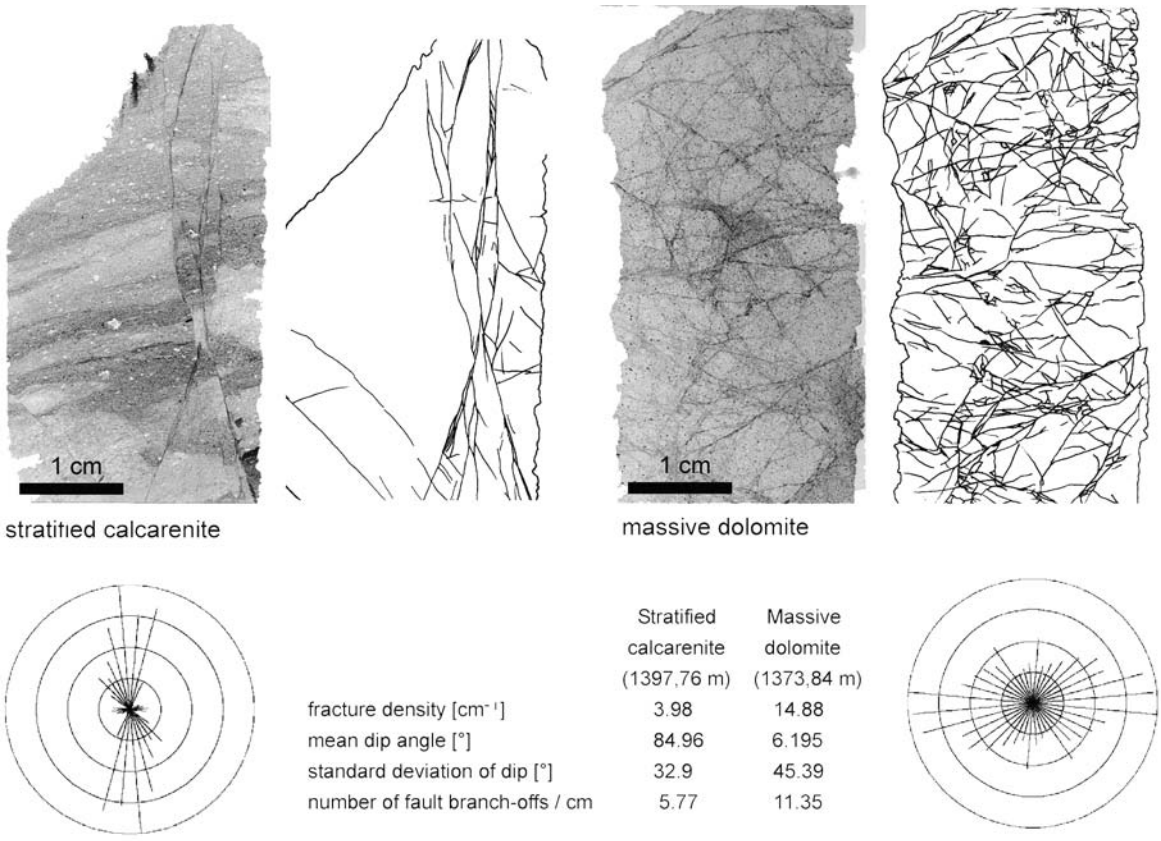

Fig. 7. Fracture analysis of a stratified calcarenite and a massive dolomite. The orientation roses display the fault orientation in 10° bins. For discussion of the differences between both rock types, see the text.

appear to be primary sediment layers enriched in organic matter. However, long-term pressure solution creep is responsible for the additional dissolution of carbonates in these layers and, hence, the selective enrichment of organic components. The fine-grained matrix of these layers consists of potassium feldspar, pyrite, apatite, and dolomite fragments, which are embedded in a matrix composed of organic matter (e.g., Fig. 12c). This organic matter shows a strong fluorescence using ultraviolet light (Fig. 12b), indicating a low maturity. Organic matter is particularly abundant in the lower part of the core (1400–1500 m).

About half of the investigated layers are viscously deformed. Abundant flow features (Fig. 12c), a well-developed foliation (Fig. 12d), and rounded fragments (Fig. 12d) resembling porphyroclasts of shear zones indicate a strong degree of ductile flattening of these mechanically weak layers by pure shear. Dolomite shows grain reduction within these zones. Platelets of iron sulfide and apatite mark the foliation. The development of a foliation suggests a long-lasting viscous response of the matrix due to lithostatic overburden loading and the onset of bitumen mobilization. The enrichment in potassium along these zones can be explained by a post-deformational fluid entrainment.

Faults and polymict clastic dikes displace rocks with layers of organic matter (e.g., Figs. 6e, 7, and 10), thereby documenting that the organic-rich layers were present before faulting and the impact event. However, a lubrication of fault planes with organic matter can also be observed. This observation, in turn, shows that a mobilization of organic matter took place afterward. The groundmass of a polymict clastic dike at 1398–1399 m is laced with mobilized organic matter (Fig. 6e). This subsequent mobilization was probably enhanced by an impact-induced thermal heat pulse on the order of 90–100 °C that can be inferred based on fluid inclusion studies, stable isotope ratios, and vitrinite measurements (Lüders et al. 2003). For the main phase of the formation of crude oil from organic matter in a non-impact setting, temperatures of 70–100 °C are required. This temperature interval correlates with a depth of 2000–3500 m, if an average geo-thermal gradient is applied (Klemme 1975). The production of natural gas extends to even higher temperatures and, thus, greater depths in a non-impact geological setting.

Estimates of the Amount of Organic Matter in Yax-1

Signs of enrichment in organic matter both as indigenous and migrated are particularly obvious in the lowermost structural unit. The concentration of organic matter is variable. Based on seven samples evaluated by organic geochemical methods, the total organic carbon contents

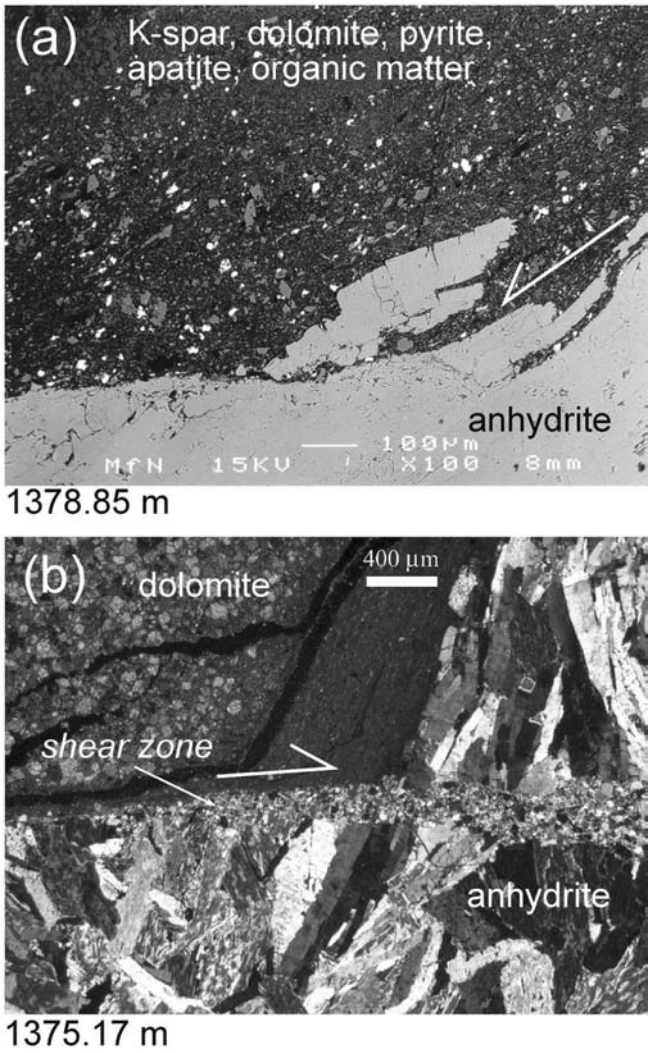

Fig. 8. Anhydrite deformation features: a) anhydrite often forms in more or less isolated pockets within dolomitic rocks and is coated by a fine-grained brownish matter. The anhydrite in this photomicrograph is present as euhedral, lepidoblastic grains. Deformation is concentrated near the rim of these anhydrite pockets. A slice of anhydrite is sheared off of the main anhydrite body. The dark zone surrounding the anhydrite pocket consists of potassium feldspar, apatite, pyrite, organic matter, and clay minerals. (SEM-BSE); b) development of a comminuted shear zone cutting through an anhydrite nodule. Grain size reduction in anhydrite most likely occurs by fracturing. However, sealing of fractures makes the deformation microstructures appear similar to those formed by dynamic recrystallization (crossed polarizers).

ranges between 0.06 and 0.66% for fine-grained carbonates and between 0.75–6.77% for darker, stained zones (Lüders et al. 2003). Most zones of increased organic content correlate with positive excursions in the K-, U-, γ-logs (Fig. 3). Lüders et al. (2003) estimated that at least 40% of the organic matter was present at the time of impact. A preliminary and rough estimate that is based on a few measurements of the total organic content (TOC) mentioned above and a macroscopic inspection of all core boxes revealed that, in total, about 13 m

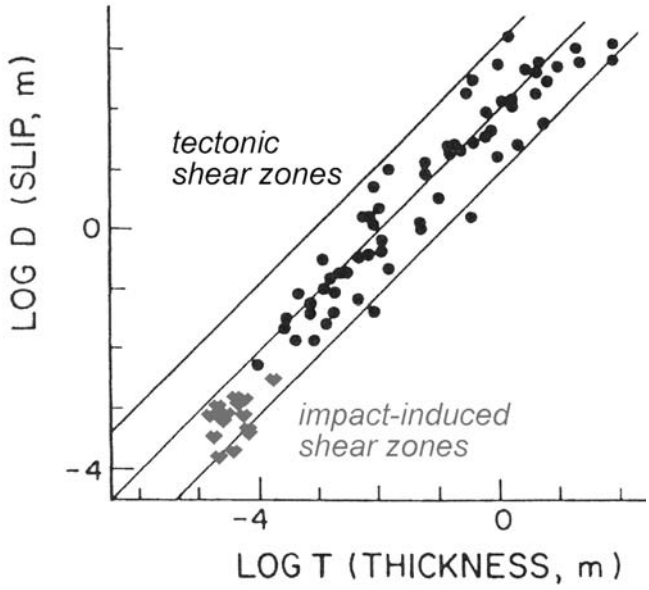

Fig. 9. Plot of log thickness of fault gouge versus log displacement of small-scale shear zones at 1399.05 m of the Yax-1 bore hole (diamonds). For comparison, data points of tectonic shear zones are displayed (Scholz 1990).

of rocks with an estimated TOC content of ~5–8% and about 32 m of rocks with a TOC content of less than ~0.8% were drilled. This roughly corresponds to a layer of 1.5 m of pure organic matter.

Impact Indicators

Indicators for shock metamorphism do not occur ubiquitously in the Cretaceous sequence. This circumstance is not surprising, as most components of the sequence were most likely situated several km outside the transient cavity. Additionally, the entire sequence consists of carbonates and sulfates for which definite shock indicators do not exist. Nevertheless, it was possible to detect unambiguous shock indicators at different levels, mostly associated with dikes. The sedimentary stratification is cut off discordantly by suevitic dikes at 909 m (Fig. 6a) and 916 m, polymict clastic dike breccias at 1314–1316 m (Figs. 6b and 10), 1341 m (Fig. 6c), and 1398–1399 m (Fig. 6e), and impact melt dikes at 1346–1350 m (Figs. 6d and 11). With the exception of the 1398–1399 m dike, all dikes analyzed by whole rock X-ray fluorescence (XRF) display a relative enrichment in potassium (Fig. 3; Schmitt et al. 2003). The dikes at 909 m and 1341 m were not analyzed for their whole rock chemical composition.

Suevitic Dikes

An intense shock metamorphic overprint occurs in the suevitic dikes at 909 m (Figs. 13a and 13b) and 916 m (Wittmann et al. 2003). These dikes contain abundant melted silicates that were quenched to glass and subsequently altered

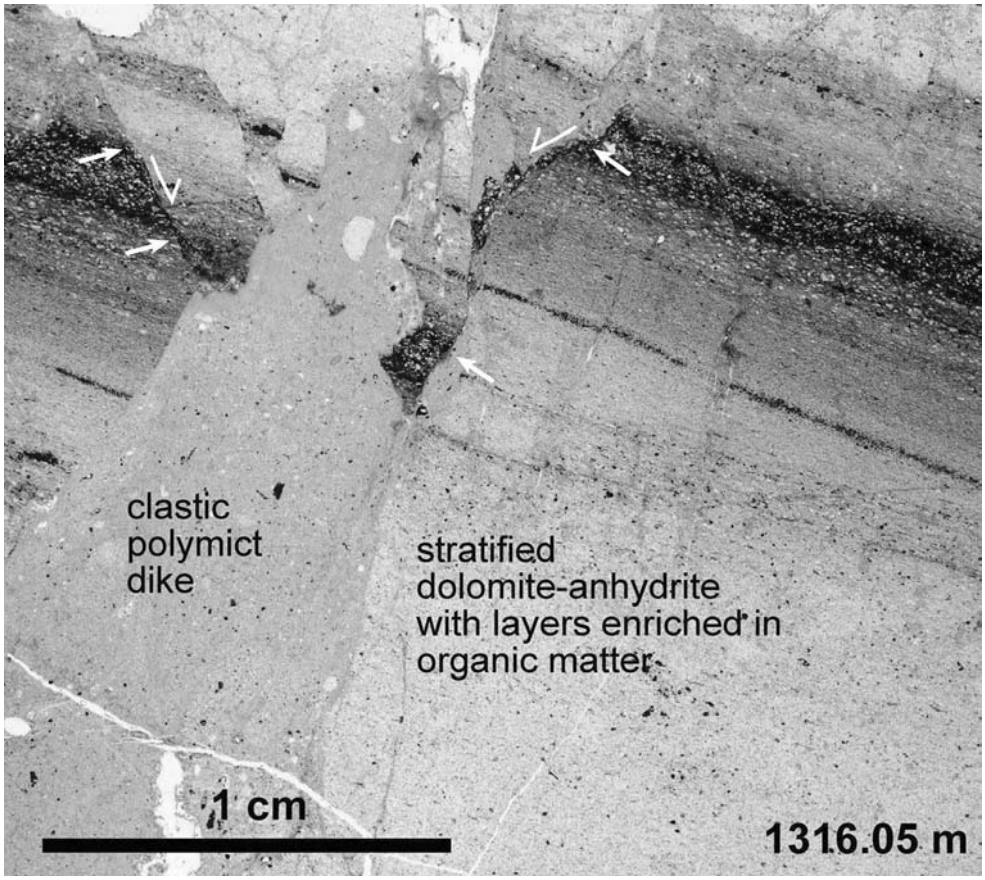

Fig. 10. Injection of a clastic polymict dike into a dolomite-anhydrite host rock that contains layers enriched in organic matter. Note the normal faults (arrows) formed co-genetically with the dike (thin section, b/w photograph).

to clay minerals and K-feldspar. Their angular to sub-angular shape shows that some silicate melt was already quenched below the glass transition temperature. However, siliceous melt was also injected into the country rock and formed thin veinlets and is now also present as interstitial fillings between euhedral calcite and dolomite crystals that may have grown in the presence of the heat pulse. This circumstance indicates that some melt was also still above the glass transition temperature during the time of emplacement. Numerous shocked quartz and feldspar grains are evidence to the impact related origin of the metamorphic overprint. A several mm-large, shocked quartz grain (Figs. 13a and 13b) with a core of diaplectic glass, surrounded by a zone in which multiple sets of planar deformation features (PDF) occur, is an exceptionally spectacular example. The PDFs in this grain terminate near a zone of tiny inclusions. This quartz grain is embedded in poly-crystalline potassium feldspar, which could be an overgrowth or a zone of coarsely (re)crystallized diaplectic glass. The suevitic dikes correspond to strong positive peaks in the K-, U-, γ-logs (ICDP/OSG/GFZ) (Fig. 3).

Impact-Melt Rock

Anastomosing vein networks of siliceous composition concentrated at 1347–1348 m (Figs. 6d and 11), which are green colored in rock samples and brownish colored in thin sections, consist of clay minerals and are interpreted as devitrified impact melt rock. The refractive indices of K-feldspar (R.I:1.518) are at the lower limit of unshocked K-feldspar. Although no other shock indicators have been found yet, the ductile flow features (Fig. 6d) and the macroscopic as well as microscopic similarity to melts of the suevitic dike at 909 m strongly suggest their impact origin. Thin veins and interstitial clay fillings are traceable down to 1374 m (Fig. 11d).

Clastic Polymict Dikes

According to Dressler (2002) and Wittmann et al. (2003), there are several polymict clastic dikes at a depth interval of 1300–1400 m cutting the stratification discordantly (Figs. 6b–6e). Although fragments of crystalline bedrock were not present in the available samples, the occurrence of granite fragments is reported in the lithological description by Dressler (2002) (ICDP/OSG/GFZ). A variety of at least 8–10 different lithologies, which include lithic types that have not been observed anywhere else in the drill core, clearly demonstrate the polymictic nature of the dikes. A shock metamorphic overprint of fragments could not be demonstrated until now.

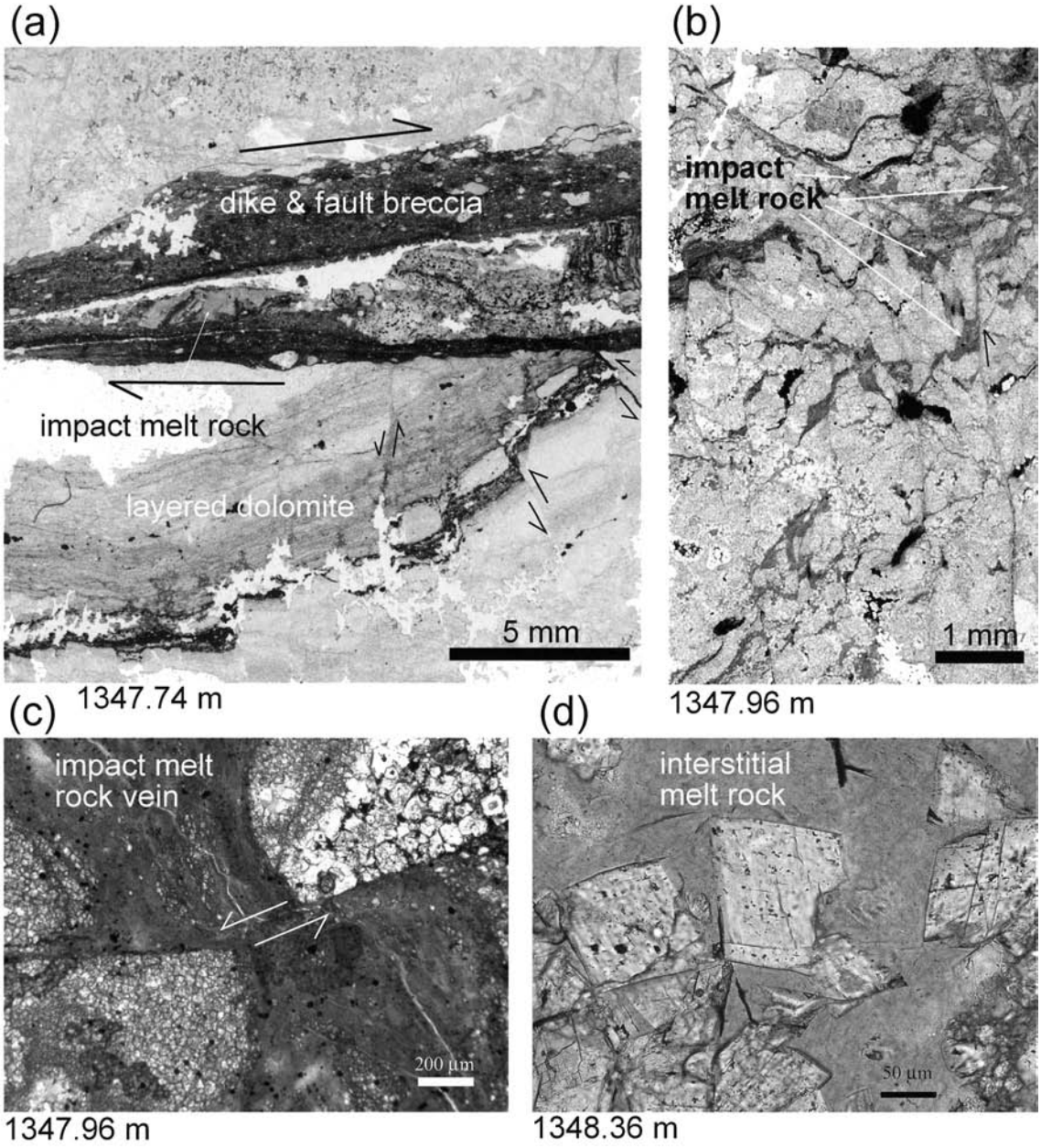

Fig. 11. a) Photomicrographs of impact melt rock dikes at 1347–1348 m. Relics of impact melt rock are incorporated in a fault breccia. The fabric and displacement on Riedel shear planes indicate a shear sense top to the left (thin section, b/w photograph); b) ductile flow features of impact melt rock (arrows) are offset by vertical faults. The impact melt lubricates the shear planes (thin section, b/w photograph); c) closeup of a single vein and fault (thin section, linear polarizers); d) melt with flow textures also occurs interstitially in brecciated dolomites. Dolomite crystals replaced the matrix melt (thin section, linear polarizers).

"Paraconglomerate"

Within the so called "paraconglomerate" at 1036–1037 m (Figs. 5a and 13c–13f) (which, in fact, is a diamictite), quartz with abundant decorated and non-decorated PDF lamellae in up to three directions (Fig. 13e) was found. Most of the shocked grains are hosted in dark-coated fragments that are connected by black veins (Figs. 13c and 13d), resembling a thin shock vein. Additionally, shocked quartz grains were discovered as common fragments within the diamictite (Fig. 13f). The diamictite itself consists of a variety of sub-rounded to angular fragments of different sizes, including anhydrite fragments, different types of limestones, relics of shells, foraminifera, chalcedony, a single crystalline plagioclase fragment, and quartz grains. They are embedded in a fine- grained dolomite matrix. The paraconglomerate resembles the detrital unit recorded in petroleum exploration drilling near the rim of the Chicxulub crater and the ejecta facies of the UNAM 5 and UNAM 7. It also shows some

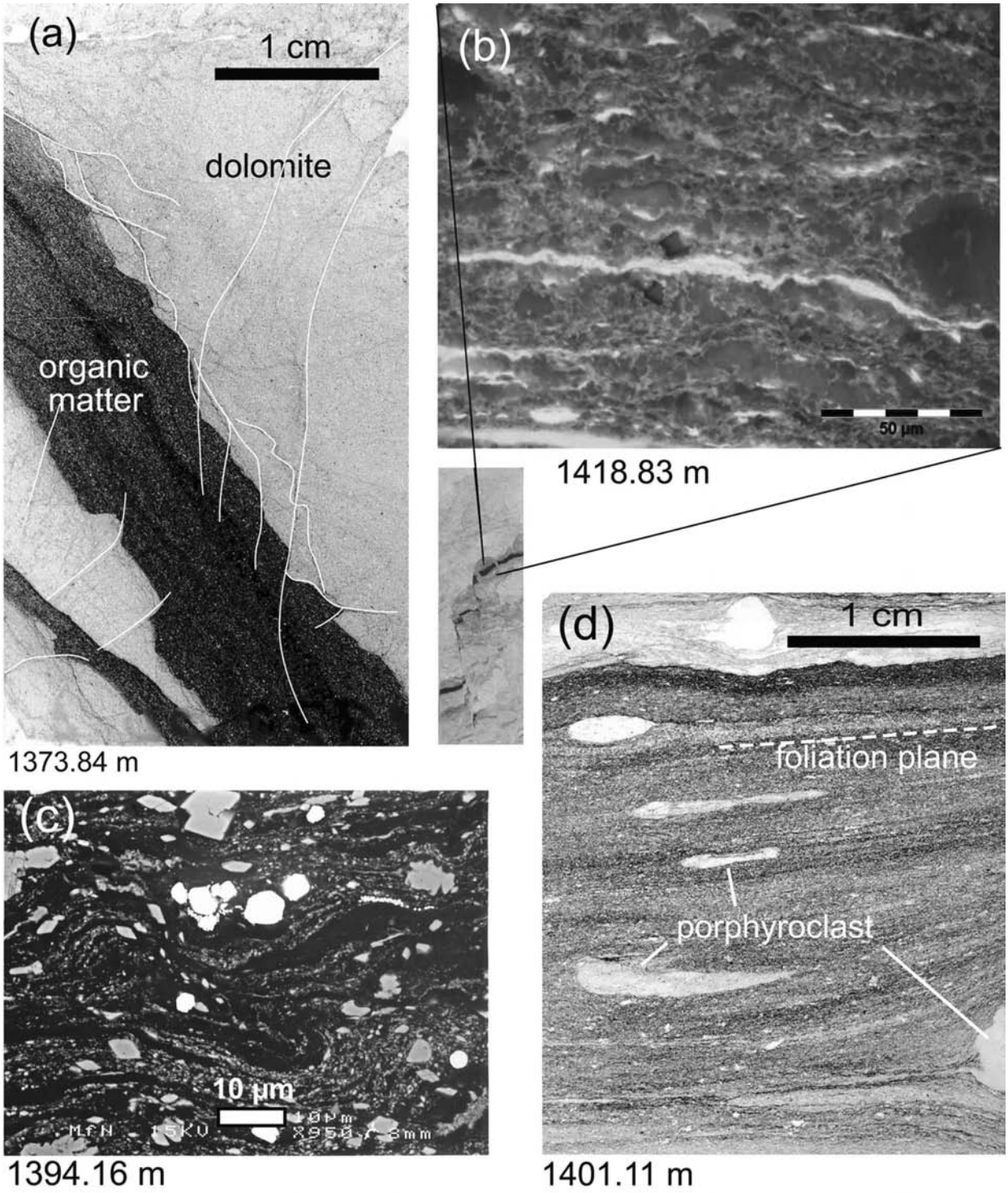

Fig. 12. Photomicrographs of layers enriched in organic matter: a) disrupted layer of organic matter in dolomite. Fault zones can be traced into the dark layer. A concentration of deformation appears to occur at the lithological boundary (thin section, b/w photograph); b) highly fluorescent low mature organic matter (alginates) in a shaly layer within limestone. The fluorescent matter appears bright, and the anorganic components (K-feldspar, dolomite) are darker (thin section, linear polarizers, UV, photograph provided courtesy of V. Lüders); c) flow textures within a dark layer enriched in organic matter. A strong alignment and high aspect ratio of fragments indicate considerable strain. Potassium feldspar, dolomite, pyrite, and apatite are the major fragments in an organic matter-clay mineral matrix. The dolomite shows grain reduction and dissolution effects within the shear zones. Iron sulfides mark the foliation. (SEM/BSE); d) the foliation plane and the stretched and rounded fragments (porphyroclasts) with symmetrical pressure shadows indicate pure shear ductile flattening of this layer, most likely induced by the lithostatic pressure (thin section, b/w photograph).

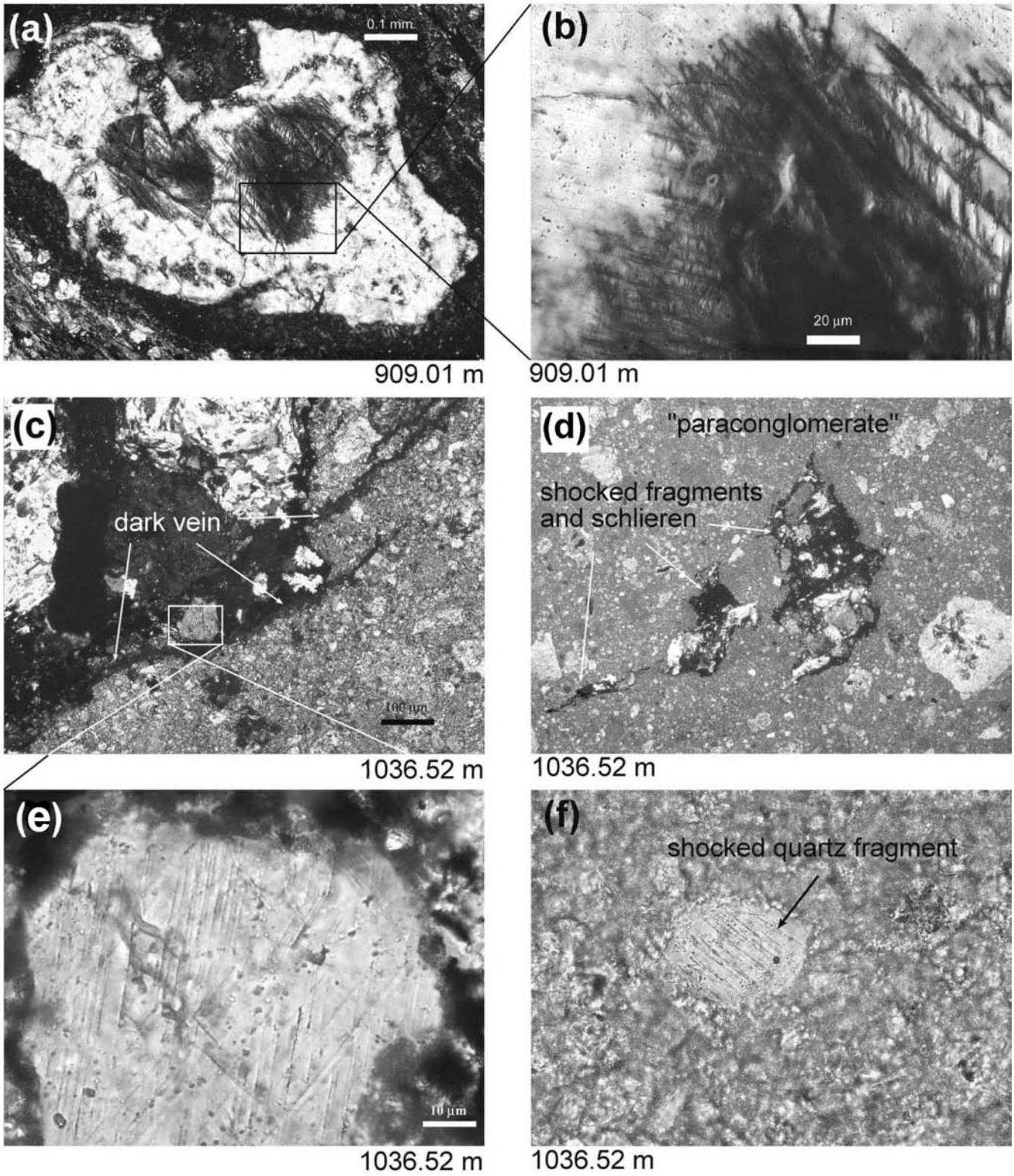

Fig. 13. Shock indicators in a suevitic dike (a) and (b) and within the paraconglomerate (c–f). Photomicrographs (a–d) are with crossed polarizers, (e–f) with linear polarizers: a) shocked quartz with a core of diaplectic glass and a rim that indicates a gradually decreased intensity of shock. The transition from core to rim is marked by a zone where abundant PDFs occur; b) close-up of (a) showing PDF lamellae; c) dark vein with shocked quartz grains marks the boundary between a large anhydrite fragment and the carbonate matrix of the diamictite; d) shocked quartz grains were mostly found in dark coated fragments that are interconnected by dark veins; e) closeup of (c) showing a quartz grain with PDF lamellae in three directions; f) shocked quartz grains also occur within the dolomite matrix of the diamictite.

similarities with the Albion formation diamictite bed found in southern Quintana Roo and Belize (Ocampo et al. 1996; Pope et al. 1999).

DISCUSSION

Formation Conditions of Faulting

Stinnesbeck et al. (2003) suggested that the Cretaceous sediments are undeformed and autochthonous. Brecciated units, such as the sequence from 1300–1400 m, and clastic dikes (personal communication) are explained to be of intraformational origin (solution collapse breccia). Solution collapse breccias are widespread on carbonate shelf platforms that experienced periods of supratidal exposure. Most commonly, solution collapse breccias are generated at subsurface levels under low lithostatic pressure. They usually display large open fractures and cavities that are eventually filled with cements. Such cavities and fractures were not observed at Yax-1 with a possible exception at 990–1000 m. In contrast, faults and fault breccias observed in the Yax-1 samples are associated with fine-grained, low-porosity fault gouges formed by shearing. To form such gouges, friction must exceed the shear strength of the particular rocks, and to do so, much higher pressures than those occurring at subsurface levels in intraformational settings are necessary.

The pure existence of 30% layered and pristine anhydrite in the Yax-1 profile and the fracturing of anhydrites (Fig. 8) shows that anhydrite dissolution and, hence, the formation of intraformational solution-collapse breccias is of subordinate importance and cannot be regarded as the main cause for faulting and brecciation in the Cretaceous sequence of the drill core.

Faults most likely formed co-genetically with the tilting of the blocks and accommodated space incompatibilities during block movements. The dominance of normal faults and the steep inclination of fault planes suggest that the principal shortening axis of the strain ellipsoid ε_1 was oriented more or less vertically during deformation. Neglecting rotational components, a vertical orientation of the principal maximum compressive stress axis σ_1 can also be derived, which indicates an extensional stress regime for the time of formation of the majority of faults. These findings fit to numerical and structural models of crater modification performed for other impact craters (e.g., Kenkmann et al. 2000). In these models, an extensional stress regime with a vertically oriented principal maximum compressive stress axis σ_1 and a radially oriented minimum compressive stress axis σ_1 is derived for a position comparable to the Yax-1 location within the crater.

Stratigraphic Comparisons with Other Bore Holes

Based on a comparison of the Yax-1 lithological profile with those of bore holes from outside the crater (T1, Y2, Y1, Y5, Y4) (López-Ramos 1975; Ward et al. 1995), some lithostratigraphical differences between these profiles are striking. For instance, unit E of Ward et al. (1995) that overlies the Cenomanian/Turonian sequence consists of shallow-platform limestones with intervals containing abundant planktonic foraminifera and rudist-bearing limestones. Such a sequence is not present at Yax-1 at this position. Additionally, for the sequence between the Cenomanian/Turonian and Maastrichtian, nearly no evaporites are reported in any of the lithological profiles of Ward et al. (1995). However, the lithological profiles by Ward et al. (1995) are based on incomplete data due to limited available corings and cuttings. Thus, evaporates could also be present at the Upper Cretaceous sequence or differ laterally across the crater. The lack of a clear correlation between Yax-1 and T-1 and other bore holes makes a stratigraphic continuity of the 615 m-thick Cretaceous sequence uncertain.

The interlayering of anhydrite/dolomite and anhydrite/limestone is typical for the lower Cretaceous units B and C of Ward et al. (1995). For Yax-1, it appears more likely that a sequence of lower Cretaceous rocks (anhydrites, dolomites/anhydrites, brecciated dolomites) is underlain by rocks of Cenomanian/Turonian age. This assumption would imply that the Cretaceous sequence is strongly disorganized. The proposed structural boundaries of the derived blocks correlate well with the lithostratigraphic boundaries defined by Stinnesbeck et al. (2003), suggesting the structurally controlled termination of lithostratigraphic units.

The drillcore's present position between the peak ring and the rim of the Chicxulub impact crater suggests that the sequence of Cretaceous rocks most likely represents a suite of displaced mega-blocks that have been slumped downward and inward from the rim of the transient crater toward their present position. If this is correct, the stratigraphic units of the Yax-1 sequence should be located at deeper crustal levels than on the surrounding undeformed platform. The Ticul-1 (T-1) bore hole (Ward et al. 1995) is located outside the crater, approximately 30 km away from Yax-1 and, hence, is the nearest locality to which Yax-1 can be compared. The Cenomanian/Turonian boundary layer in T-1 probably occurs at a depth of ~800–950 m (Ward et al. 1995) in comparison to 1495–1455 m in the Yax-1 bore hole. This circumstance would indicate a downward movement of ~650 m of the upper Cretaceous blocks during crater modification, which is consistent with models of crater collapse. Using particle trajectory of crater collapse models (e.g., Melosh and Ivanov 1999; Kenkmann et al. 2000), these downward movements may correspond to an inward movement on the order of several km. As mentioned above, the middle part of the Yax-1 Cretaceous sequence (from 1142–1462 m) that dominantly consists of anhydrites, interlayered anhydrites/dolomites, and anhydrites/calcarenites could probably correlate with lower Cretaceous sequences (unit b and c in Ward et al. [1995]. At

T-1, these units were drilled at a depth of >1500 m, thus indicating an upward movement of these units in the Yax-1 section. While a detailed explanation of this upward motion cannot be given due to the one-dimensional exposure in the bore hole, it has to be taken into account that particle trajectories during crater collapse are generally complex and do not follow simple radial downward-inward paths. For instance, a local uplift of rocks can occur within radial folds (Kenkmann 2002) and radial transpression ridges (Kenkmann and von Dalwigk 2000) during convergent flow.

Comparison with Other Impact Craters

When comparing the position of the Yax-1 bore hole inside the Chicxulub crater with the smaller but relatively well-preserved Ries impact structure, the locality would correspond to the so called mega-block zone (e.g., Angenheister and Pohl 1969) where monomict and polymict impact breccias of different shock levels and size are present. At larger impact craters like Siljan (65 km in diameter), the locality would correspond to the complex ring syncline where downfaulted blocks of Paleozoic carbonates are present. These blocks show minor to moderate internal deformation, but they are evidently displaced for several km (Kenkmann and von Dalwigk 2000).

Degree of Shock Metamorphism in the Mega-Block Suite

It was shown that definitive indicators for shock metamorphism are restricted to the dikes within the Cretaceous sequence with the exception of the so called paraconglomerate. The occurrence of shocked quartz in fragments of this diamictite provokes a discussion on its formation. Four lines of explanations are principally possible: a) the paraconglomerate is an impact breccia similar to the detrital units and ejecta facies of the Pemex and UNAM bore holes that contain shocked material; b) shock veins intruded the paraconglomerate; c) the entire Cretaceous sequence has suffered shock pressures in excess of 10 GPa, which leads to PDF formation in quartz but no visible shock features in carbonates and sulfates. As quartz is absent otherwise, the only visible tracers of this shock can be seen in the paraconglomerate; d) the shocked quartz fragments of the paraconglomerate have formed during an earlier Cretaceous impact event when this strata was deposited. The entire paraconglomerate is then interpreted as an impact-induced deposition.

The paraconglomerate shows a more or less stratiform contact to the foot wall and hanging wall units. The hanging wall contact also displays indication for graded bedding. If the paraconglomerate represents an analogue to the detrital units and ejecta facies of the Pemex and UNAM bore holes as proposed in (a), one would expect sharp contacts to the surrounding Cretaceous mega-blocks. Undeformed shells of foraminifera found in the paraconglomerate do not indicate a shock-metamorphic overprint. However, similar foraminifera clasts are also present in the sorted suevite units at 794–823 m, suggesting some potential of foraminifera fossils for indicating a shock metamorphic overprint. If the paraconglomerate is an analogue to the diamictites from outside the crater, this could be regarded as evidence that large parts of the Cretaceous sequence belong to the excavated deposits and not to the displaced crater floor. Explanation (b) is supported by the local occurrences of dark coatings and ductile flow features that surround most of the shocked grains and resemble injected shock veins (Fig. 13d). However, we also found shocked quartz grains and exotic fragments as common fragments in the matrix. Explanation (c) would imply that the 10 GPa pressure isobar encounters the Cretaceous sequence at a distance 60 km from the impact center. This is in strong contrast to numerical models that merely suggest a pressure of 0.6 GPa at this distance (Ivanov, personal communication). To achieve a mean shock pressure of ~10 GPa at 60 km from the impact center, a projectile diameter of ~60 km would be necessary, leading to a crater of ~700–1000 km in diameter. Such a diameter, of course, is in contradiction to any geophysical data that constrain Chicxulub with respect to its size. This could probably indicate that the Cretaceous sequence is composed of individual mega-blocks that stem from various regions, some of which must have been a lot closer to the crater center. The low potential for carbonate and anhydrite rocks to record a shock metamorphic overprint was experimentally confirmed by Martinez et al. (1995) and Deutsch et al. (2003). Explanation (d) is possible in principle, but it seems not very likely and straightforward to postulate a second impact when finding shock features within a well-documented impact crater.

Preliminary Kinematic Model

The analysis of deformation features of the Cretaceous sequence of Yax-1 shows that these rocks originally must have been located outside the transient cavity before the crater collapse affected the sequence (Fig. 14). This fact gives an upper limit for the size of the Chicxulub transient cavity of 120 km in diameter, which reconfirms earlier estimates based on geophysical, numerical, and scaling investigations. The Cretaceous rocks have been tracked to within 40 km of the crater center along the major seismic line (Fig. 1b) (Morgan and Warner 1999; Snyder and Hobbs 1999). Restoring this sequence to its pre-collapse position, the size of the excavated zone can be defined. Accepting the mostly used diameter of 90–100 km for the transient cavity (e.g., Kring 1995), the bulk of the Cretaceous rocks of Yax-1 are estimated to originally have been located ~15 km away from the transient crater rim where a ubiquitous shock metamorphic overprint is not to be expected. They successively moved inward during crater

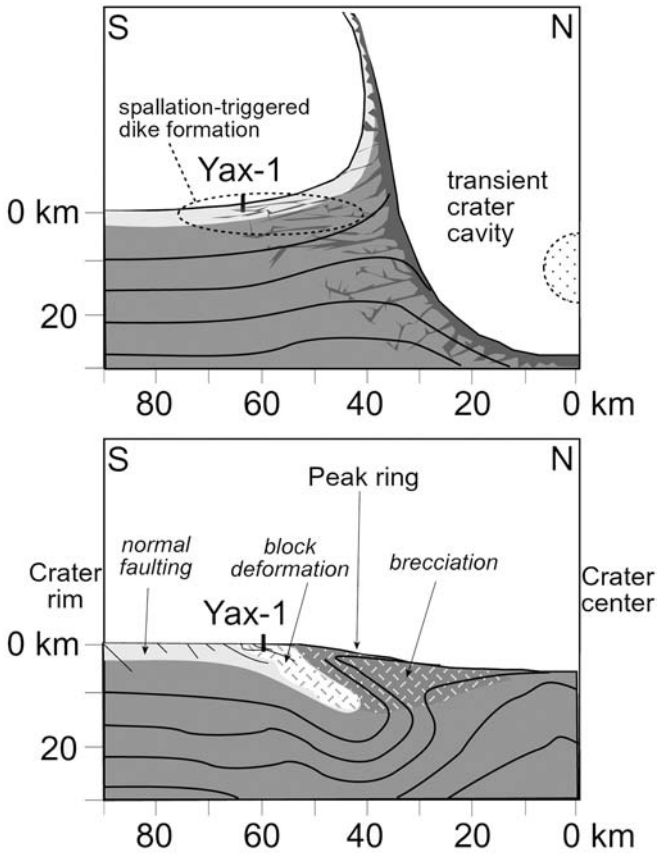

Fig. 14. The upper sketch shows a generalized proposed locality for the bulk blocks constituting Yax-1 when the transient crater cavity had reached its maximum depth. The bore hole is at a position where interference of the shock wave with the free surface may have triggered weak spallation. The latter favors the formation of sub-horizontal detachments and the injection of dikes into the host rock. The lower sketch shows the structure after crater modification had ceased. The intensity of deformation in the crater floors of complex impact craters decreases with increasing distance from the crater center and is indicated by an increasing size of displaced blocks. We suggest that total brecciation in Chicxulub correlates with the extent of the peak ring. The formation of blocks and mega-blocks are typical for the localiy of Yax-1, while in more distal parts of the crater, discrete faulting is the dominant expression of the impact induced deformation. Crater shape and dimensions are adopted from a numerical model of Ivanov et al. (2003).

collapse to their present position 60 km south-southwest from the crater center. The structural and lithostratigraphic data support discrete movements of blocks that led to abrupt changes in the dip angle and dip azimuth of the bedding planes. The azimuth data of the dip-meter log show that some blocks are tilted toward the center of the structure, thereby indicating a centerward and downward displacement. We postulate that the middle part of the sequence (1142–1450 m), which probably has a lower Cretaceous age, was squeezed upward and in between upper Cretaceous sequences as a consequence of convergent inward flow. Limited bending and folding of blocks is suggested by the dip-meter log data. The suevitic dikes near the top of the Cretaceous sequence were probably injected from the ground-surged suevite by a drag-induced delamination of the uppermost Cretaceous sediments. The decoupling of mechanical blocks along weak bedding planes and the injection of dikes was probably supported by spallation forces (Fig. 14). Cross cutting relationships suggest that the impact melt rock dikes at 1347–1348 m have formed at an early stage of cratering, most likely the compression and early excavation stage. Breccias, faults, and clastic dikes may have started to form during the growth of the transient cavity, but the majority of faults are eventually formed to accommodate the inward and downward movements of blocks during gravity driven collapse of the transient cavity.

An alternative interpretation of the emplacement process of the Cretaceous sequence is given by Stöffler et al. (2004): the sequence is explained as a stack of displaced mega-blocks that were transported more or less horizontally and radially outward at the final stage of the transient cavity excavation process and moved somewhat back inward during the subsidence of the outer parts of the transient crater. In other words, the Cretaceous sequence is considered as a part of the ejecta. This interpretation is in agreement with estimates of the ejecta thickness, which, according to results of numerical models, should be some 800 to 1000 m thick (Stöffler et al. 2004). It would also explain the occurrence of the paraconglomerate diamictite as ejecta facies.

The Fate of Organic Matter During the Impact

We showed that abundant organic matter was present before the impact within the Cretaceous sediments. This stimulates the question of what happened to the organic matter during the impact event. Based on the assumption that the organic content of the Yax-1 sequence is typical for the entire Chicxulub area, an estimation of the amount of organic matter that was excavated during the impact event is possible. If a transient cavity size of 100 km in diameter (area: 7850 km^2) is assumed, about 12 km^3 of organic matter would be excavated during the growth of the transient cavity. This conservative estimate merely considers the organic matter volume of a pile of 615 m of Cretaceous sediments as drilled in the Yax-1 borehole. The amount of organic matter is particularly high in the lower structural unit that was not entirely drilled. Furthermore, when considering a thickness of 3000 m for the sedimentary pile, the total amount of excavated organic matter can reach >100 km^3. The fate of the excavated kerogen, bitumen, or oil depends on the achieved temperature and pressure—that means, on its position with respect to the impact center. Thermal cracking of organic matter may have occurred in the hot vapor plume and below the impact melt sheet. A hint to such reactions was found in the Yax-1 borehole (Lüders et al. 2003). Ethane and butane were trapped in fluid inclusions and indicated a localized

thermal peak of >250 °C. Potential devastating and toxic effects of organic matter on the past climate have to be unraveled. Pope et al. (1997) have calculated the climatic effects of volatiles being released to the stratosphere by the impact and proposed that the greenhouse warming effect caused by impact-generated CO_2 was not significant. The contribution of CO_2 released from organic matter appears negligibly small in comparison to that of vaporized carbonates. To assess the role of organic matter in detail, the global K/T soot layers, which are so far explained by global wildfires (Anders et al. 1986; Gilmour et al. 1990), may play a dominant role and should be reinspected in light of an impact into an organic matter-bearing sedimentary sequence. The presence of fullerenes at several K/T boundary localities (Heymann et al. 1999) appears important in this respect, since they could form as a result of a pyrolysis of organic matter in a hot vapor plume.

CONCLUSIONS

The degree of tilting and faulting of the Cretaceous sequence of the Yax-1 bore hole was analyzed making use of the 360°-core scans and dip-meter log data. In accordance to lithological information, these data suggest that the sedimentary profile is composed of a number of individual structural units that are tilted and moved with respect to each other. Three main units and nine sub-units were discriminated. Brittle deformation is most intense at the top of the sequence and at the depth interval of 1300–1400 m. Within these zones, suevitic dikes, polymict clastic dikes, and impact melt rock dikes occur. The degree of brittle deformation depends on lithology; massive dolomites are affected by penetrative faulting, while stratified calcarenites and bituminous limestones display localized faulting. The deformation pattern and the inferred state of stress are consistent with a collapse scenario of the Chicxulub transient crater cavity. It is believed that parts of the Cretaceous sequence have originally been located outside the transient crater cavity and were successively included in the crater-forming process when they moved centerward to their present position between the peak ring and the crater rim. The analysis of the deformation microstructure indicates that a shock metamorphic overprint is restricted to the dike injections with an exception of the so called paraconglomerate. Whether the lack of ubiquitous shock metamorphism in the Cretaceous rocks reflects the absence of sensitive shock indicators or a strongly attenuated shock wave is in question. The presence of abundant organic matter in the Yax-1 core was evidently present before the impact and stimulated an estimation of the amount of excavated organic material during the cratering process. The release of large amounts of organic matter into the atmosphere should be critically tested as a potential cause for global mass extinction.

Acknowledgments–This work was supported by the German Science Foundation (DFG) grants KE 732/8–1, 8–2. We thank the Chicxulub Scientific Drilling Project of the International Continental Drilling Program and the Universidad Nacional Autónoma de México for providing the Yax-1 drill core samples. We are also indebted to the Chicxulub Research Group at Humboldt-University, including the collegues of the GFZ-Potsdam, V. Lüders, B. Horsfield, B. Mingram, and B. A. Ivanov (Russian Academy of Science) for providing data and constructive discussions. Thanks to the operational support team (OSG) of the ICDP, in particular, R. Conze and J. K. M. Kück, for helping with the borehole logging data analysis. Sean Gulick, Kevin Pope, and Jo Morgan provided very constructive reviews of the manuscript.

Editorial Handling—Dr. Joanna Morgan

REFERENCES

Anders E., Wolbach W. S., and Lewis R. S. 1986. Cretaceous extinctions and wildfires. *Science* 234:261–264.

Angenheister G. and Pohl J. 1969. Die seismischen Messungen im Ries von 1948–1969. *Geologica Bavarica* 61:304–326.

Brittan J., Morgan J., Warner M., and Marin L. 1999. Near-surface seismic expression of the Chicxulub impact crater. In *Large meteorite impacts and planetary evolution II,* edited by Dressler B. O. and Sharpton V. L. Special Paper 339. Boulder: Geological Society of America. pp. 269–279.

Christeson G., Nakamura Y., and Buffler R. 1999. Upper crustal structure of the Chicxulub impact crater from wide-angle ocean bottom seismograph data. In *Large meteorite impacts and planetary evolution II,* edited by Dressler B. O. and Sharpton V. L. Special Paper 339. Boulder: Geological Society of America. pp. 291–305.

Christeson G. L., Morgan J. V., and Warner M. R. 2001. Deep three-dimensional structure of the Chicxulub impact crater (abstract #1728). 32nd Lunar and Planetary Science Conference.

Dressler B. O. 2002. Summary of the lithological report for ICDP/Chicxulub-Yax-1, ICDP/OSG GeoForschungsZentrum Potsdam.

Dressler B. O., Sharpton V. L., Morgan J., Buffler R., Moran D., Smit J., Stöffler D., and Urrutia J. 2003. Investigating a 65-Ma-old smoking gun: Deep drilling of the Chicxulub impact structure. *Eos Transactions* 84:125, 130.

Deutsch A., Langenhorst F., Hornemann U., and Ivanov B. A. 2003. On the shock behavior of anhydrite and carbonates—Is post-shock melting the most important effect? Examples from Chicxulub (abstract #4080). 3rd International Conference on Large Meteorite Impacts. CD-ROM.

Ebbing J., Janle P., Koulouris J., and Milkereit B. 2001. 3-D gravity modeling of the Chicxulub impact structure. *Planetary and Space Science* 49:599–609.

Gilmour I., Wolbach W. S., and Anders E. 1990. Major wildfires at the Cretaceous/Tertiary boundary. In *Catastrophes and evolution: Astronomical foundations,* edited by Cube S. V. M. Cambridge: Cambridge University Press. pp. 195–213.

Heymann D., Chibante L. P. F., Brooks R. R., Wolbach W. S., Smit J., Korochantsev A., Nazarov M. A., and Smalley R. E. 1996. Fullerenes of possible wildfire origin in Cretaceous-Tertiary boundary sediments. In *The Cretaceous-Tertiary event and other catastrophes in Earth history,* edited by Ryder G., Fastovsky D., and Gartner S. Special Paper 307. Boulder: Geological Society of America. pp. 453–464.

Hildebrand A. R., Penfield G. T., Kring D. A., Pilkington M., Camargo-Zanoguera A., Jacobson S. B., and Boynton W. V. 1991. Chicxulub crater: A possible Cretaceous-Tertiary boundary impact crater on the Yucatán Peninsula, Mexico. *Geology* 19:867–871.

Hildebrand A. R., Pilkington M., Ortiz-Aleman C., Chavez R. E., Urrutia-Fucugauchi J., Connors M., Graniel-Castro E., Camara-Zi A., Halpenny J. F., and Niehaus D. 1998. Mapping Chicxulub crater structure with gravity and seismic reflection data. In *Meteorites: Flux with time and impact effects,* edited by Grady M. M., Hutchison R., McCall G. J. H., and Rothery D. London: Geological Society Special Publications. pp. 155–176.

Kenkmann T. 2002. Folding within seconds. *Geology* 30:231–234.

Kenkmann T. and von Dalwigk I. 2000. Radial transpression ridges: A new structural feature of complex impact craters. *Meteoritics & Planetary Science* 35:1189–1202.

Kenkmann T., Ivanov B. A., and Stöffler D. 2000. Identification of ancient impact structures: Low-angle normal faults and related geological features of crater basements. In *Impacts and the early Earth, Lecture notes in Earth sciences,* edited by Gilmour I. and Koeberl C. Berlin: Springer-Verlag. pp. 271–309.

Kenkmann T., Wittmann A., Scherler D., and Schmitt R. T. 2003. Deformation features of the Cretaceous units of the ICDP Chicxulub drillcore Yax-1 (abstract #1368). 34th Lunar and Planetary Science Conference.

Kenkmann T., Wittmann A., Scherler D., and Stöffler D. 2003. The Cretaceous sequence of the Chicxulub Yax-1 drillcore. What is impact derived? (abstract #4075). 3rd International Conference on Large Meteorite Impacts.

Klemme H. D. 1975 Geothermal gradients, heat flow, and hydrocarbon recovery. In *Petroleum and global tectonics,* edited by Fischer A. G. and Judson S. Princeton: Princeton University Press. pp. 251–304.

Kring D. A. 1995. The dimensions of the Chicxulub impact crater and impact melt sheet. *Journal of Geophysical Research* 100:16979–16986.

López-Ramos E. 1975. Geological summary of the Yucatán Peninsula. In *Ocean basins and margins, The Gulf of Mexico and Caribbean,* edited by Nairn A. E. M. and Stehli F. G. New York: Plenum Press. pp. 257–282.

Lüders V., Horsfield T., Kenkmann T., Mingram B., and Wittmann A. 2003. Hydrocarbon and aqueous fluids in Cretaceous sediments of the ICDP-Chicxulub drill core Yax-1 (abstract #1378). 34th Lunar and Planetary Science Conference.

Martinez I., Deutsch A., Schärer U., Ildefonse P., Guyot F., and Agrinier P. 1995. Shock recovery experiments on dolomite and thermodynamical calculations of impact induced decarbonation. *Journal of Geophysical Research* 100:15465–15476.

Melosh H. J. 1997. Multi-ringed relevation. *Nature* 390:439–440.

Melosh H. J. and Ivanov B. A. 1999. Impact crater collapse. *Annual Review of Earth and Planetary Sciences* 27:385–415.

Morgan J. and Warner M. 1999. Morphology of the Chicxulub impact: Peak-ring crater or multi-ring basin? In *Large meteorite impacts and planetary evolution II,* edited by Dressler B. O. and Sharpton V. L. Special Paper 339. Boulder: Geological Society of America. pp. 281–290.

Morgan J. and Warner M. 1999. Chicxulub: The third dimension of a multi-ring impact basin. *Geology* 27:407–410.

Morgan J., Warner M., Collins G. S., Melosh H. J., and Christeson G. L. 2000. Peak-ring formation in large impact craters: Geophysical constraints from Chicxulub. *Earth and Planetary Science Letters* 183:347–354.

Morgan J., Warner M., Brittan J., Buffler R., Camargo-Zanoguera A., Christeson G., Denton P., Hidebrand A., Hobbs R., Macintyre H., Mackenzie G., Maguire P., Marin L., Nakamura Y., Pilkington M., Sharpton V., Snyder D., Suarez G., and Trejo A. 1997. Size and morphology of the Chicxulub impact crater. *Nature* 390:472–476.

Ocampo A. C., Pope K. O., and Fischer A. G. 1996. Ejecta blanket deposits of the Chicxulub crater from Albion island, Belize. In *The Cretaceous-Tertiary event and other catastrophes in Earth history,* edited by Ryder G., Fastovsky D., and Gartner S. Special Paper 307. Boulder: Geological Society of America. pp. 75–88.

Pilkington M., Hildebrand A. R., and Ortiz-Aleman C. 1994. Gravity and magnetic field modeling and structure of the Chicxulub crater, Mexico. *Journal of Geophysical Research* 99:13147–13162.

Pope K. O., Ocampo A. C., Kinsland G. L., and Smith R. 1996. Surface expression of the Chicxulub crater. *Geology* 24:527–530.

Pope K. O., Baines K. H., Ocampo A. C., and Ivanov B. A. 1997. Energy, volatile production, and climatic effects of the Chicxulub Cretaceous/Tertiary impact. *Journal of Geophysical Research* 102:21645–21664.

Pope K. O., Ocampo A. C., Fischer A. G., Alvarez W., Fouke B. W., Webster C. L., Vega F. J., Smit J., Fritsche A. E., and Claeys P. 1999. Chicxulub impact ejecta from Albion island, Belize. *Earth and Planetary Science Letters* 170:351–364.

Schmitt R. T., Wittmann A., and Stöffler D. 2004. Geochemistry of drill core samples from Yaxcopoil-1, Chicxulub impact crater, Mexico. *Meteoritics & Planetary Science* 39:979–1001.

Scholz C. H. 1990. *The mechanics of earthquakes and faulting.* Cambridge: Cambridge University Press. 439 p.

Sharpton V. L., Marín L. E., Carney J. L., Lee S., Ryder G., Schuraytz B. C., Sikora P., and Spudis P. D. 1996. A model of the Chicxulub impact basin based on evaluation of geophysical data, well logs, and drill core samples. In *The Cretaceous-Tertiary event and other catastrophes in Earth history,* edited by Ryder G., Fastovsky D., and Gartner S. Boulder: Geological Society of America. pp. 55–74.

Snyder D. B. and Hobbs R. W. 1999. Deep seismic reflection profiles across the Chicxulub crater. In *Large meteorite impacts and planetary evolution II,* edited by Dressler B. O. and Sharpton V. L. Special Paper 339. Boulder: Geological Society of America. pp. 263–268.

Stinnesbeck W., Keller G., Adatte T., Harting M., Istrate G., Kramar U., and Stüben D. 2003. The Chicxulub impact based on the Yaxcopoil-1 drillhole and other events in the K/T transition in Mexico, Central America and the Caribbean. Proceedings, Schwerpunktkolloqium IODP-ICDP Mainz. 3 p.

Stöffler D., Ivanov B. A., Hecht L., Kenkmann T., Schmitt R. T., Salge T., Schönian F., Tagle R., Weseler S., and Wittmann A. 2003. Origin and emplacement of the impact formations at Chicxulub, Mexico, with special emphasis on the Yax-1 deep drilling (abstract #4092). 3rd International Conference on Large Meteorite Impacts, Nördlingen.

Stöffler D., Artemieva N. A., Ivanov B. A., Hecht L., Kenkmann T., Schmitt R. T., Tagle R. A., and Wittmann A. 2004. Origin and emplacement of the impact formations at Chicxulub, Mexico, as revealed by the ICDP deep drilling Yaxcopoil-1 and by numerical modeling. *Meteoritics & Planetary Science*. This issue.

Wittmann A., Kenkmann T., Schmitt R. T., and Stöffler D. 2003. Polymict clastic dykes in the "mega-block" sequence of the ICDP Chicxulub drill core Yax-1 (abstract #1386). 34th Lunar and Planetary Science Conference.

Wittmann A., Kenkmann T., Schmitt R. T., Hecht L., and Stöffler D. 2004. Impact-related dike breccia lithologies in the ICDP drill core Yaxcopoil-1, Chicxulub impact structure, Mexico. *Meteoritics & Planetary Science* 39:931–954.

Ward W. C., Keller G., Stinnesbeck W., and Adatte T. 1995. Yucatán subsurface stratigraphy: Implications and constraints for the chicxulub impact. *Geology* 23:873–876.